

# Multivariate geostatistical modeling of the spatial sediment distribution in a large scale drainage basin, Upper Rhone, Switzerland

Anna Schoch <sup>a,\*</sup>, Jan Henrik Blöthe <sup>a</sup>, Thomas Hoffmann <sup>a,b</sup>, Lothar Schrott <sup>a</sup>

<sup>a</sup> Department of Geography, University of Bonn, Germany

<sup>b</sup> Federal Institute of Hydrology, BfG, Koblenz, Germany



## ARTICLE INFO

### Article history:

Received 23 July 2017

Received in revised form 17 November 2017

Accepted 30 November 2017

Available online 6 December 2017

### Keywords:

Sediment budget

Sediment storage

Predictive modeling

Rhone Basin

## ABSTRACT

There is a notable discrepancy between detailed sediment budget studies in small headwater catchments ( $<10^2 \text{ km}^2$ ) focusing on the identification of sedimentary landforms in the field (e.g. talus cones, moraine deposits, fans) and large scale studies ( $>10^3 \text{ km}^2$ ) in higher order catchments applying modeling and/or remote sensing based approaches for major sediment storage delineation.

To bridge the gap between these scales, we compiled an inventory of sediment and bedrock coverage from field mapping, remote sensing analysis and published data for five key sites in the Upper Rhone Basin (Val d'Illiez, Val de la Liène, Turtmannal, Lötschental, Goms;  $360.3 \text{ km}^2$ , equivalent to 6.7% of the Upper Rhone Basin). This inventory was used as training and testing data for the classification of sediment and bedrock cover. From a digital elevation model ( $2 \times 2 \text{ m}$  ground resolution) and Landsat imagery we derived 22 parameters characterizing local morphometry, topography and position, contributing area, and climatic and biotic factors on different spatial scales, which were used as inputs for different statistical models (logistic regression, principal component logistic regression, generalized additive model). Best prediction results with an excellent performance (mean AUROC:  $0.8721 \pm 0.0012$ ) and both a high spatial and non-spatial transferability were achieved applying a generalized additive model. Since the model has a high thematic consistency, the independent input variables chosen based on their geomorphic relevance are suitable to model the spatial distribution of sediment.

Our high-resolution classification shows that  $53.5 \pm 21.7\%$  of the Upper Rhone Basin are covered with sediment. These are by no means evenly distributed: small headwaters ( $<5 \text{ km}^2$ ) feature a very strong variability in sediment coverage, with watersheds drowning in sediments juxtaposed to watersheds devoid of sediment cover. In contrast, larger watersheds predominantly show a bimodal distribution, with highest densities for bedrock (30–40%) being consistently lower than for sediment cover (60–65%). Earlier studies quantifying sedimentary cover and volume focus on the broad glacially overdeepened Rhone Valley that accounts for c. 9% of our study area. While our data support its importance, we conservatively estimate that the remaining 90% of sediment cover, mainly located outside trunk valleys, account for a volume of  $2.6\text{--}13 \text{ km}^3$ , i.e. 2–16% of the estimated sediment volume stored in the Rhone Valley between Brig and Lake Geneva. Furthermore, our data reveal increased relative sediment cover in areas deglaciated since the Little Ice Age, as compared to headwater regions without this recent glacial imprint. We therefore conclude that sediment storage in low-order valleys, often neglected in large scale studies, constitutes a significant component of large scale sediment budgets that needs to be better included into future analysis.

© 2017 Elsevier B.V. All rights reserved.

## 1. Introduction

The topography of the earth's surface is created by the interplay of climate, tectonics, and geomorphic processes (e.g. Molnar and England, 1990; Whipple, 2009). This interaction of endogenic and exogenic processes created mountain ranges with steep topographic gradients featuring some of the highest sediment fluxes on earth. The

transport of eroded material through a geomorphic system has been described as a sediment cascade connecting source to sink, involving a chain of subsystems dynamically linked by the transfer of mass or energy (Chorley and Kennedy, 1971; Caine, 1974; Slaymaker, 1991; Milliman and Syvitski, 1992; Burt and Allison, 2010).

Many high-mountain geomorphic systems are considered to be out of equilibrium or in a transient state in terms of the external driving forces, i.e. a shift from glacial to interglacial conditions, because the response to environmental changes is not immediate but buffered and delayed (Phillips, 2003; Hoffmann, 2015). Several cycles of ice advance and retreat during Pleistocene glaciations created a distinct topography

\* Corresponding author at: Meckenheimer Allee 166, 53115 Bonn, Germany.

E-mail address: [anna.schoch@uni-bonn.de](mailto:anna.schoch@uni-bonn.de) (A. Schoch).

in many mountain systems (Penck, 1905) and produced, eroded and transported vast amounts of sediment (e.g. Hallet et al., 1996; Montgomery, 2002; Schlüchter, 2004). Furthermore, glacial erosion created overdeepened valleys (e.g. Preusser et al., 2010; Prasicek et al., 2014; Haeberli et al., 2016), hanging valleys (e.g. Valla et al., 2010b), and glacial cirques (e.g. Hooke, 1991; Evans, 2006) that potentially retain vast amounts of sediment (Hoffmann et al., 2013). Despite substantial potential energy in mountain environments, sediment flux in large river systems is frequently disconnected from alpine headwaters, due to intermittent storage along the flow path from the bedrock source to large sedimentary sinks in major alpine valleys (e.g. Otto et al., 2009; Hoffmann et al., 2013; Messenleh et al., 2014). Thus, the sediment delivery to the outlet is by no means a simple and consistent relationship between drainage area and sediment yield as only a small fraction of sediment eroded within the catchment is delivered to its outlet (Hoffmann et al., 2013). Therefore, detailed studies on the spatial distribution of sediments are needed to explain the discrepancy (Walling, 1983; Phillips, 1986; Church and Slaymaker, 1989; de Vente et al., 2007; Hinderer, 2012; Fryirs, 2013) and to better understand sediment routing in alpine environments (Otto et al., 2008).

Moreover, the spatial pattern of sediment storage has important implications for the prediction, mitigation and management of natural hazards (Zimmermann and Haeberli, 1993; Glade, 2005), the analysis of seismic wave propagation (Allen and Wald, 2009), and the management of hydropower reservoirs in mountain regions.

Sediment storage and flux along sediment cascades is controlled by scale specific system properties including (1) scale dependency of processes, (2) emergent phenomena arising at larger spatial scales, (3) feedbacks associated with process interactions at various scales, and (4) spatial heterogeneity (of objects) (Zhang et al., 2004). Thus, results from sediment budgets at small spatial scales cannot be simply transferred (Phillips, 1999; Slaymaker, 2006; Tunnicliffe and Church, 2011) and call for new approaches for the investigation of sediment storages on large scales.

The distribution of sediment storages has been investigated on different spatial and temporal scales (comprehensive review by Hinderer, 2012). Detailed studies are mainly available for small scale drainage basins ( $<10^2 \text{ km}^2$ ) (e.g. Otto et al., 2009; Götz et al., 2013; Messenleh et al., 2014), whereas studies in larger drainage basins ( $>10^3 \text{ km}^2$ ) rather focus on large scale sedimentary landforms such as valley fills (e.g. Hinderer, 2001; Straumann and Korup, 2009). Very few of the large scale studies included different sediment storage types in their budgets (e.g. Jäckli, 1957; Jordan and Slaymaker, 1991; Phillips, 1991; Tunnicliffe and Church, 2011; Tunnicliffe et al., 2012). Thus, the scaling of erosion, transport and storage and their controlling factors are insufficiently understood (Otto et al., 2008; Tunnicliffe and Church, 2011) because tributaries and headwaters are often portrayed to act as sediment sources without substantial sediment storage (Schumm, 1977; Hinderer, 2001). However, the significance of headwaters and smaller catchments as sediment storage areas has been reported in various studies (e.g. Otto et al., 2009; Götz et al., 2013; Hoffmann et al., 2013). Systematically neglecting these small scale sediment storages might introduce notable error into sediment budgets (Hoffmann, 2015). Thus, treating sediment storage as a black box in large drainage basins is problematic and needs to be addressed.

Therefore, knowledge on the spatial pattern of sediment storage and the mobility of material along the sediment cascade in a large drainage basin are imperative to a better understanding of transient landscape evolution and postglacial sediment evacuation and connectivity from and within the tributaries of large scale drainage basins. While direct geomorphic mapping in the field and from remote sensing data has shown to be useful in small scale studies (e.g. Schrott et al., 2003; Hoffmann et al., 2013), it is not suitable for large scale drainage basins. Predictive spatial models have been used to regionalize geomorphic processes or landforms mapped in smaller areas (e.g. Luoto and Hjort, 2005; Marmion et al., 2008; Brenning, 2009).

Here we use predictive modeling to incorporate the hitherto under-represented sediment storage in headwaters into a regional assessment of sediment distribution, "a major challenge of geomorphic studies in mountain environments" (Hoffmann, 2015, p. 625). To address this shortcoming, we investigate the spatial distribution of sediment storage in a large alpine drainage basin, the Upper Rhone Basin (URB), and aim to:

- model the spatial distribution of sediment cover in the URB using a combined field-based and statistical modeling approach,
- analyze the quality of the model outcome and the effects of input data on this in a large scale geomorphic system, and
- interpret the modeling results in a geomorphic context with respect to the general pattern, the topographic position of sediment storages, the relevance of sediment storage in recently deglaciated areas and the spatial variability of sediment storage on different scales.

We apply a hierarchical approach where the spatial distribution of sediment storage is studied in five key sites in catchments up to a scale of  $10^2 \text{ km}^2$ . This data is then used to statistically model the spatial distribution of sediment storage in the large scale URB using logistic regression, principal component logistic regression, and generalized additive models.

## 2. Study area

The URB is located in the Swiss Alps between the Rhone Glacier and Lake Geneva, and is the largest inner alpine basin with a size of c.  $5400 \text{ km}^2$  (Fig. 1). The Rhone Valley with a total length of c. 160 km dissects the western Swiss Alps with a general southwest trend, along regional tectonic structures. The valley abruptly changes to a north-northwest direction at Martigny. It shows an asymmetry whereby the tributaries draining the area north of the main valley are smaller than the tributaries in the south. The drainage basin is a closed system for suspended and clastic sediment transport with Lake Geneva acting as a sediment sink. The basin is located between 372 and 4634 m asl, with dozens of peaks reaching elevations of  $>4000 \text{ m}$ .

### 2.1. Tectonic and geological setting

The bedrock geology of the URB is dominated by three major tectonic units: the Helvetic unit, the Penninic unit and the crystalline basement bedrock (Fig. 2). For a detailed overview of the architecture of the Alps we refer to Schmid et al. (2004). The southwest oriented Rhone Valley marks a major tectonic boundary (Rhone-Simplon fault) between the Penninic and the Helvetic units. The Penninic units cover the largest area of the catchment mainly located south of the Rhone and consist of Penninic basement nappes and Mesozoic sediments. Thus, folding involved the crystalline basement rocks (mainly metamorphic rocks: gneiss, schists, and metasedimentary rocks). The Helvetic and Ultrahelvetic nappes are part of the former continental margin and located north of the Rhone-Simplon fault, i.e. the Rhone Valley. The unit is dominated by nappes consisting of (meta)sedimentary rocks (mainly Mesozoic and Tertiary limestone dominated cover nappes). The crystalline basement bedrock includes the Aar Massif, the largest of the Swiss massifs, the Gotthardt Massif (Allochthonous massifs and Infra-Penninic crystalline nappes) occurring upstream of Brig and in the Goms and Aletsch region, as well as the Mt. Blanc and Aiguilles Rouges Massifs underlying the area near Martigny and the Mt. Blanc region. The lithology comprises mainly granitic rocks as well as gneiss, schists and metagranitoids (Schmid et al., 2004).

### 2.2. Pleistocene glaciation, Little Ice Age and current glacier extent

The topography is strongly impacted by the Pleistocene glaciations and thus characterized by U-shaped valleys, cirques, hanging valleys

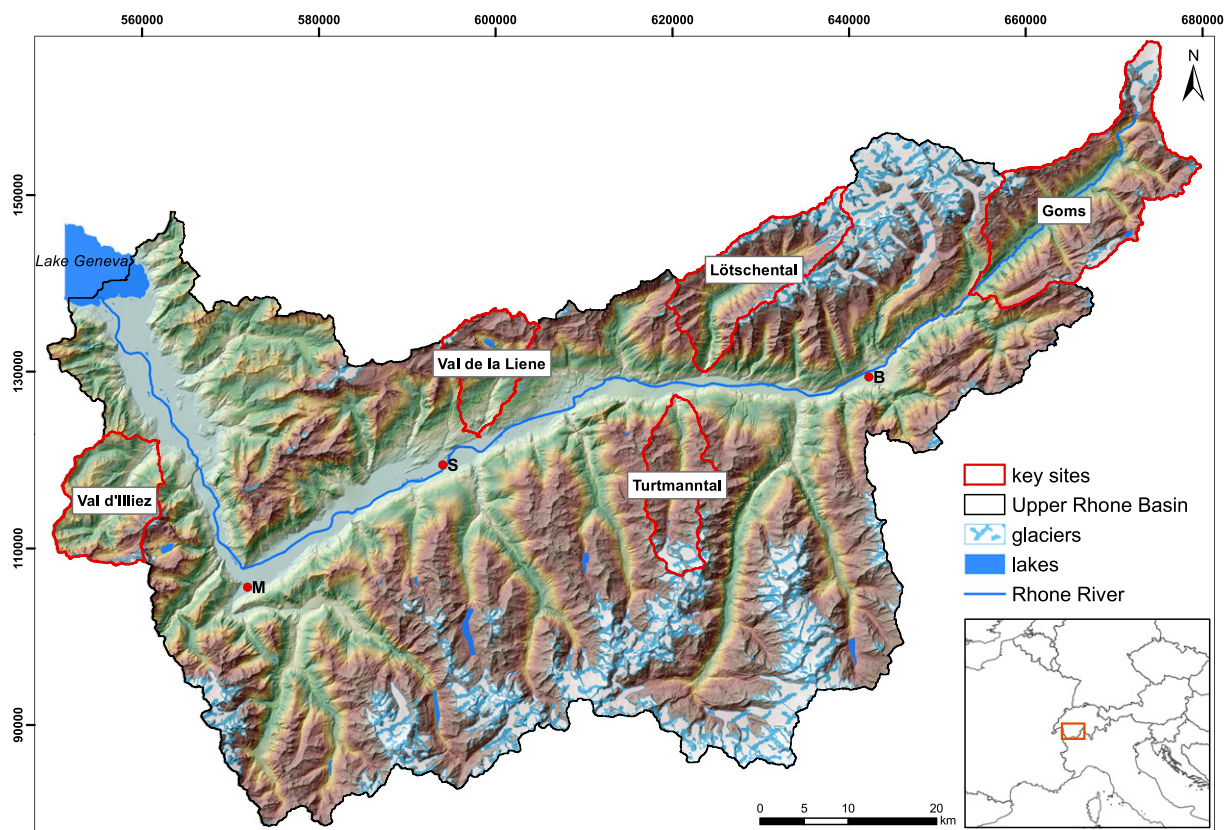


**Fig. 1.** Location of study area and key sites within the Upper Rhone Basin (M = Martigny, S = Sion, B = Brig). Glacier extent from Swiss glacier inventory 2010 (Fischer, 2013). Lakes classified based on digital elevation model (DEM) with a semi-automated surface classification model (Bowles and Cowgill, 2012). (DEM from swisstopo, projection: CH1903).

and steep peaks. Glacial erosion produced a high-mountain landscape with peaks over 4000 m and glacial overdeepenings up to 1000 m (Pfiffner et al., 1997). During the Last Glacial Maximum (LGM) the glaciers in the study area were influenced by at least four centers of ice accumulation: the Rhone ice dome, the Aletsch ice field, the southern Valais icefield and the Mt. Blanc region (Kelly et al., 2004). The Rhone ice dome with radial outflow following the pre-existing valley system but also flowing over the high passes was located in the headwaters of the Rhone Valley (Florineth and Schlüchter, 1998). The LGM Rhone Glacier filled the Rhone Valley, overflowed onto the foreland and was the main component of the LGM transection glaciers in the western Alps, an interconnected system of valley glaciers. It reached a thickness of as much as 2300 m near Martigny (Kelly et al., 2004). The Rhone Glacier extended into the alpine foreland after 30 ka and deglaciation (retreat from LGM position) began in  $21.1 \pm 0.9$  ka and ice collapse already initiated between 16.8 and 17.4 ka (Ivy-Ochs et al., 2004; Ivy-Ochs et al., 2006). Currently the glacially conditioned landscape is adjusting to fluvial conditions through e.g. fluvial incision (Valla et al., 2010b), mass wasting (McColl, 2012), and sediment transport (Church and Slaymaker, 1989), i.e. the landscape is in a transient state (Brunsden and Thornes, 1979; Schlunegger and Norton, 2013). The adjustment from a glacial to a fluvial landscape is prominent at the so called transition zones between the Rhone Valley and the tributaries, often forming hanging valleys. Transition zones are characterized by knickpoints, steep gradients and V-shaped valleys. They are dominated by river incision and unstable slopes. Within the URB, these knickpoints are located close to the trunk stream because lithologies with low erodibility are widespread (e.g. Schlunegger and Hinderer, 2003; Norton et al., 2010; Valla et al., 2010a; Valla et al., 2010b).

Compared to other regions in the Alps, glaciers are widespread in the URB due to high elevations and precipitation from (north)westerly and south/southwesterly atmospheric circulation patterns (Kelly et al.,

2004). Approximately 569 km<sup>2</sup> (c. 10.6%) of the land surface was covered with glacial ice in 2010 (Fischer, 2013; Fischer et al., 2014). The highest glacier cover is located in the Aletsch region, in the southern part of the study area, the Valais Alps and especially the Matteringtal, the Mont Blanc massif and in the Goms region with the Rhone Glacier (Penninic unit and crystalline basement rock). In the Helvetic unit the glacial cover is comparably low. This is conditioned by the substantially higher elevations in the Penninic unit and crystalline basement rock. During the Little Ice Age (LIA) c. 929 km<sup>2</sup> were covered with glacial ice (Maisch, 2000), hence the deglaciated areas since 1850 comprise 360 km<sup>2</sup> within the URB. The glaciers within the study area lost c. 39% of their areal extent within the time period 1850–2010.

### 2.3. Key sites

Five key sites, Val d'Illiez, Val de la Liene, Turtmannatal, Lötschental and Goms, have been selected to reflect the heterogeneity of the URB and its tributaries (Fig. 1, Table 1). They cover all three major tectonic units (Fig. 2), many lithologies exposed within the study area and the full width of surface morphology, relief, Pleistocene glacial imprint and contemporary glacial cover are represented. Each key site spans across different spatial scales. Mean elevations of the key sites vary between 1650 and 2500 m, however the surface morphology is comparable with mean slope gradients between 26 and 32%. Within the URB a total area of 360.3 km<sup>2</sup> of bedrock and sediment was mapped in the five key sites corresponding to 6.7% of the total basin area.

### 3. Methods

Our main goal is to investigate the spatial distribution of sediment and bedrock within the URB at various scales. The distribution of sediment and bedrock was mapped in five key sites on a spatial scale of

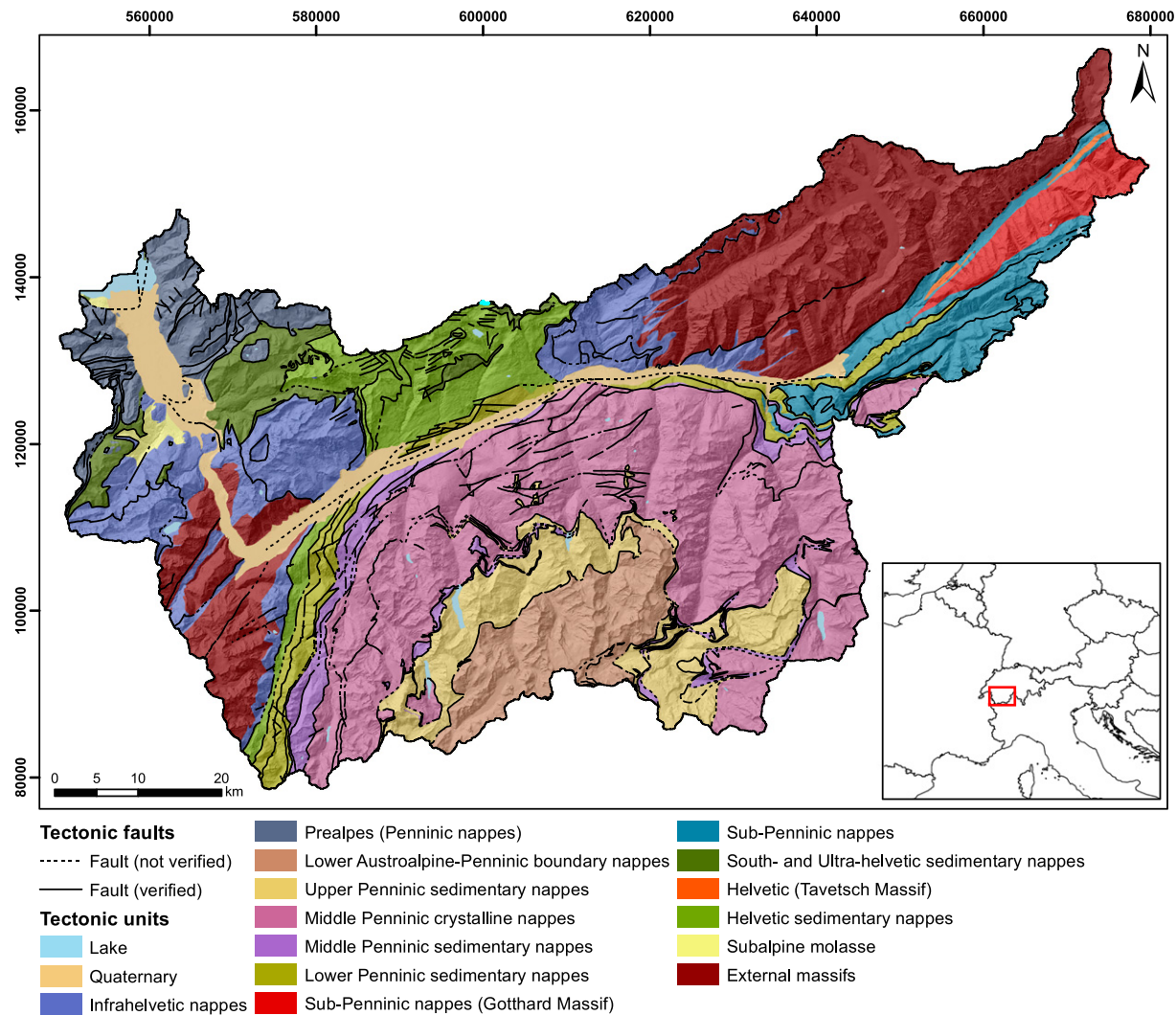


**Fig. 2.** Simplified geologic map of the Upper Rhone Basin showing the major litho-tectonic units and tectonic faults (data from ©swisstopo geologic map 1:500,000, DEM from swisstopo, projection: CH1903).

up to  $>200 \text{ km}^2$  and then upscaled to the large scale URB using a statistical predictive modeling approach (Fig. 3). We focus on a distinction between bedrock and sediment in general, which encompasses all sediment accumulation forms, including as valley fills, fans, debris cones, terraces, talus deposits, moraines, and debris mantled slopes. A requirement for the application of a predictive model is a statistical relation between the studied objects and the available spatial information (predictive variables) to create a spatial probability model (Schlummer

et al., 2014). The final output is a detailed map of the spatial sediment/bedrock distribution in the URB.

### 3.1. Dataset

An inventory of sediment storage and bedrock, compiled from field mapping, remote sensing imagery analysis and published data, was created for the five key sites and used as training and testing data for the

**Table 1**

Characteristics of the five key sites in the Upper Rhone Basin. Glacier extent from Swiss glacier inventory 2010 (Fischer, 2013). Erodibility after Kühni and Pfiffner (2001).

Key site	Total area [km <sup>2</sup> ]	Min. elevation [m]	Max. elevation [m]	Mean elevation [m] $\pm$ 1SD	Glacier cover [%]	Lake cover [%]	Mean slope gradient [%] $\pm$ 1SD	Lithology	Erodibility	Absolute and relative mapped area [km <sup>2</sup> /% of URB]	
										Bedrock	Sediment
Val d'Illiez	135.59	427	3254	1647 $\pm$ 472	1.22	0.02	29.18 $\pm$ 13.64	Flysch, limestone	Medium	25.87/0.48	27.49/0.51
Val de la Liène	90.90	506	3248	1921 $\pm$ 627	1.22	0.94	26.11 $\pm$ 14.21	Limestone	Medium	28.25/0.52	26.88/0.50
Turtmanntal	107.95	638	4152	2517 $\pm$ 552	10.81	0.14	29.14 $\pm$ 13.12	Metamorphic rocks	Low	40.91/0.76	18.05/0.34
Lötschental	164.73	649	3962	2393 $\pm$ 584	14.23	0.04	32.31 $\pm$ 14.52	Granites and metamorphic rocks	Low	57.43/1.07	21.52/0.40
Goms	233.27	1309	3629	2305 $\pm$ 484	11.66	0.43	28.92 $\pm$ 14.43	Granites and metamorphic rocks	Very low - low	51.12/0.95	62.78/1.17
Total										203.58/3.78	156.72/2.91

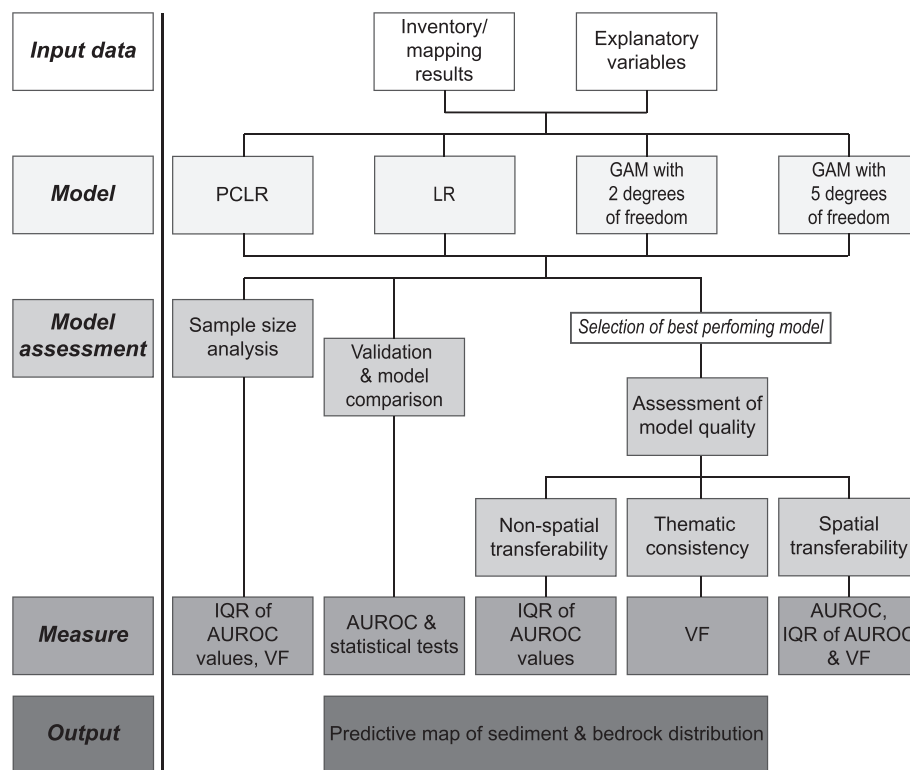


**Fig. 3.** Flow chart of applied statistical methods to model the spatial distribution of sediment cover in the large scale Upper Rhone Basin based on geomorphic maps of sediment storages and bedrock cover from key sites (PCLR = principal component logistic regression model, LR = logistic regression model, GAM = generalized additive model, AUROC = area under the receiver operating characteristics curve, IQR = interquartile range of the AUROC values, VF = variable selection frequency).

classification of sediment and bedrock cover applied to the whole URB. Sediment storage and bedrock were mapped in the field, complemented by the interpretation of satellite imagery available on GoogleEarth, as well as a digital elevation model (DEM, 2 × 2 m resolution, swissALTI3D, ©swisstopo). The geomorphic map of the hanging valleys from the Turtmannal was taken from Otto et al. (2009) and extended to the trunk valley. In total, an area of 360.3 km<sup>2</sup> was mapped, equivalent to 6.7% of the total area of the URB (Table 1). Mapped areas were classified into a binary raster (1 = bedrock, 0 = sediment/non-bedrock). Furthermore, the Swiss glacier inventory 2010 was used (Fischer, 2013; Fischer et al., 2014) to exclude areas covered by glaciers with a minimum area of 0.01 km<sup>2</sup>. Lakes were classified based on the DEM data and a semi-automated surface classification model (Bowles and Cowgill, 2012). Both, glacier and lake areas were masked from the input data for modeling.

We compiled a set of predictor (independent) variables that are anticipated to explain the differences in surface morphology, topography and position, characteristics of the contributing area as well as biotic and climatic differences between sediment storages and bedrock. Since all input parameters need a comparable resolution, no data on lithology, erodibility or other rock mechanics or tectonics related input parameters could be included directly in the modeling approach, since no high resolution data for these parameters is available for the entire study area. The chosen input parameters conceptually explain the differences between bedrock and sediment on different scales (Table 2). These 22 variables were derived from the high-resolution DEM and orthorectified Landsat 5 TM and 7 ETM + scenes following the approach by Brenning (2009), who combined process-related terrain attributes and multispectral remote-sensing data. Data were processed using the raster package in the open-source statistical software R (Hijmans, 2014; r-project.org), SAGA GIS (saga-gis.org) and Esri ArcGIS (esri.com).

Local surface morphology predictor variables include slope gradient, roughness, curvature and the topographic wetness index (Beven and

Kirkby, 1979; O'Callaghan and Mark, 1984). Topography and position are represented by the elevation, slope gradient, roughness, curvature (the latter three from 25 m DEM), aspect, normalized distance to ridge, hypsometric index, local relief and vertical distance to channel network. Aspect variables were split into directional components resulting in "east-exposedness" and "north-exposedness" variables (Brenning, 2009). Normalized distance to ridge was calculated by semi-automatically extracting the ridgelines from the watershed boundaries (2nd–5th order watershed based on 1 km<sup>2</sup> stream head threshold) and the stream network (same threshold) representing the relative position within the sediment cascade (Messenzehl et al., 2014). The contributing area was delineated based on the D8-flow algorithm (O'Callaghan and Mark, 1984) and log transformed due to the extremely skewed distribution of the data (Brenning, 2009). The mean slope of the contributing area was calculated using a slope weighted flow accumulation divided by the unweighted flow accumulation. Climatic and biotic factors encompass solar radiation and the normalized difference vegetation index (NDVI) respectively. Landsat scenes (path 195, row 28, acquisition dates in June, July, August, September, one from October, see Supplementary material A) were used to compute the maximum NDVI for each cell.

### 3.2. Predictive modeling

We applied and compared three different statistical classification techniques, a logistic regression model (LR), a principal component logistic regression model (PCLR) and a generalized additive model (GAM). Classifiers are used to match a pixel based on the independent variables and the observation of the mapping results to a class (1 = bedrock, 0 = sediment/non-bedrock), i.e. they predict the probability of class membership to class 1. Further, we evaluated the predictive power of each classifier to quantify which model predicts the spatial distribution of sediment storages in the URB best. LR and PCLR are

**Table 2**

Candidate variables representing local morphometry, topography and topographic position, contributing area, climatic and biotic factors on different scales.

Name	Variable	Description	Formula	Scale
<i>Local morphometry</i>				
PLC10	Plan curvature	Calculated from resampled 10 m DEM (bilinear interpolation) due to noisy character of small scale curvature (Heckmann et al., 2014)		Small
PRC10	Profile curvature	Calculated from resampled 10 m DEM (bilinear interpolation) due to noisy character of small scale curvature (Heckmann et al., 2014)		Small
CUR10	Overall curvature	Calculated from resampled 10 m DEM (bilinear interpolation) due to noisy character of small scale curvature (Heckmann et al., 2014)		Small
SLP	Slope gradient [%]	Calculated from original 2 m DEM		Small
ROU	Roughness	Standard deviation of slope [°] in a 3 × 3 cell moving window, calculated from original 2 m DEM		Small
TWI	Topographic wetness index	Calculated from original 2 m DEM A... upslope contributing area A (D8-flow algorithm) B... slope raster in radians (Beven and Kirkby, 1979; O'Callaghan and Mark, 1984)	$\text{TWI} = \ln\left(\frac{A}{\tan(\beta)}\right)$	Small
<i>Topography and position</i>				
DEM	Digital elevation model	Elevation [m]		Large
SLP25	Slope gradient [%]	Calculated from resampled 25 m DEM (bilinear interpolation)		Meso
ROU25	Roughness	Calculated from resampled 25 m DEM (bilinear interpolation)		Meso
PLC25	Plan curvature	Standard deviation of slope [°] in a 3 × 3 cell moving window		Meso
PRC25	Profile curvature	Calculated from resampled 25 m DEM (bilinear interpolation)		Meso
CUR25	Overall curvature	Calculated from resampled 25 m DEM (bilinear interpolation)		Meso
ASP_NS	North-exposedness	Cosine of the original aspect raster [°]		Small
ASP_EW	East-exposedness	Sine of the original aspect raster [°]		Small
NDR	Normalized distance to ridge	Relative position within the sediment cascade (ridgeline: NDR = 1, channel: NDR = 0) (Messenleh et al., 2014)		Large
REL40	Local relief	Calculated in moving window with a radius of 40 m Z... elevation [m]	$\text{REL40} = Z_{\max} - Z_{\min}$	Meso
HI40	Hypsometric index	Calculated in moving window with a radius of 40 m Z... elevation [m] (Brocklehurst and Whipple, 2004)	$\text{HI40} = \frac{Z_{\text{mean}} - Z_{\min}}{Z_{\max} - Z_{\min}}$	Meso
VDC	Vertical distance to channel network	DEM... digital elevation model [m] $CN_{int}$ ... interpolated surface from the channel network [m]	$\text{VDC} = \text{DEM} - CN_{int}$	Large
<i>Contributing area</i>				
ACCLOG	Size of the contributing area [m <sup>2</sup> ]	D8-flow algorithm, log transformed (O'Callaghan and Mark, 1984; Brenning, 2009)		Large
ACCSLP	Mean slope [%] of the contributing area	Slope weighted D8-flow algorithm divided by unweighted flow accumulation		Large
<i>Climatic and biotic factors</i>				
SR	Solar radiation	Potential annual incoming solar radiation 2015 [Wh m <sup>-2</sup> ]		Small
NDVI	Normalized difference vegetation index	Landsat TM scenes converted to Landsat ETM + values (Vogelmann et al., 2001) Atmospheric and illumination corrections applied to receive top of atmosphere reflectance values (Chander et al., 2009).		Meso

parametric techniques, i.e. they can only model linear relations between dependent and independent variables, while a GAM is a non-parametric classifier allowing non-linear relationships. For each model a dataset consisting of equal number of cases (bedrock pixels) and controls (sediment/non-bedrock pixels) was used (event/non-event ratio of 1) (Heckmann et al., 2014). In all three modeling approaches, a combined forward and backward stepwise model selection based on the Akaike Information Criterion (AIC) is applied (Akaike, 1974; Atkinson et al., 1998; Brenning, 2005; Petschko et al., 2014).

### 3.2.1. Logistic regression model

LR are one of the most widely applied models in geomorphology (Brenning, 2005) to predict system properties described by a binary variable. The LR is a generalized linear model based on the logistic function. The logit or log-odds is calculated by:

$$Y = \log\left(\frac{p(X)}{1-p(X)}\right) = \beta_0 + \beta_1 X_1 + \dots + \beta_n X_n \quad (1)$$

where Y is the dependent (response) binary variable (bedrock vs. sediment), p(X) is the probability of bedrock occurrence,  $\beta$  are the coefficients, X are the independent input variables and n is the number of independent input variables (Atkinson et al., 1998; Hosmer et al., 2013).

The coefficients of the model are estimated using a randomly sampled training dataset. Only non-collinear predictor variables should be used in a LR. Multicollinearity makes the interpretation of the model results difficult. Thus, multicollinearity was tested using the variance inflation factor for all 22 candidate variables (Aguilera et al., 2006; James et al., 2013). Overall curvature (calculated from 10 and 25 m DEM), local relief and topographic wetness index were excluded from the dataset used in the LR and the GAM (see Supplementary material B) because variance inflation factor values larger than 10 indicate a problematic amount of collinearity (Heckmann et al., 2014). The remaining 18 variables, all having variance inflation factor values below 5, were used as independent variables.

### 3.2.2. Principal component logistic regression

PCLR is firstly a principal component analysis (PCA) to produce independent principal components (PCs) as predictors to prevent multicollinearity between the input datasets. Secondly, the PCs are used as input variables in a LR (Hengl et al., 2004; Aguilera et al., 2006; James et al., 2013; Hoffmann et al., 2014; Messenleh et al., 2017). The key idea is that a smaller number of PCs are sufficient to explain most of the variability of the dataset and thus the relation to the response variable. Furthermore, the reduction of input variables in the model can mitigate overfitting (Aguilera et al., 2006; James et al.,

2013). The PCA was performed with the psych package in R (Revelle, 2015; r-project.org). To analyze the PCs more easily and intuitively the factors must be rotated. The varimax rotation is an orthogonal rotation of the PC axes. Thus, the PCs have large or small loadings on any of the input variables (Kaiser, 1958). The number of PCs used in the PCLR was limited by a visual analysis of the knickpoint in an eigenvalue plot. Although eigenvalues under 1 are equal to the information explained by a single variable, these minor PCs with little explained variance may still be correlated to the dependent variable (Aguilera et al., 2006).

The PCA was performed by selecting random samples from all five key sites for all 22 input variables. From each key site c. 1% of all mapped pixels were selected (c. 140,000 to 290,000 pixels per site). The large dataset produced for this study is ideal for statistical modeling as the selection of only a small fraction of all data prevents overfitting and allows validation (James et al., 2013). The stability of the PCA was tested by applying a full PCA ten times to independent datasets and investigating the variance.

### 3.2.3. Generalized additive model

A GAM is considered a good compromise between the non-linear flexibility of machine learning techniques and the linear predictions of LR (Brenning, 2005; Brenning, 2008; Goetz et al., 2011). GAMs extend the LR by allowing linear and non-linear transformations of the independent variables utilizing smoothers but keeping the additive structure that is easily interpreted. Thus, they are more data-driven while the LR is more model-driven (Hastie and Tibshirani, 1990; Brenning, 2008; Hastie et al., 2009).

In a GAM the response variable is not modeled directly, but as in the "ordinary" LR the logit of the occurrence probability of bedrock  $p(X)$  is the result:

$$Y = \log\left(\frac{p(X)}{1-p(X)}\right) = \beta_0 + \beta_1 f_1 X_1 + \dots + \beta_n f_n X_n \quad (2)$$

where  $Y$  is the dependent (response) binary variable (bedrock vs. sediment),  $f$  are non-parametric smoothing functions,  $\beta$  are the coefficients,  $X$  are the independent input variables and  $n$  is the number of independent input variables (Hastie and Tibshirani, 1990). Two variations of the GAM were applied. In the GAM2df each variable can be selected as a linear (not transformed) or a non-linear (transformed with a smoothing spline with two degrees of freedom), or not at all included in the model. In the second version GAM5df the transformed variables may be entered not at all, untransformed or transformed with up to five degrees of freedom, thus allowing more flexibility of the model. GAM modeling was conducted with the gam package in R (Hastie, 2015; r-project.org).

### 3.3. Validation and assessment of model quality

We applied non-spatial and spatial validation approaches (using ten times a 25-fold validation) to investigate quality and transferability of the models (Brenning, 2012). Spatial validation tests a model in an independent site, thus accounting for the presence of spatial autocorrelation. This is not incorporated in the more widely used non-spatial equivalent (Brenning, 2012). Furthermore, we analyzed the thematic consistency (Goetz et al., 2011; Petschko et al., 2014) and the impact of spatial heterogeneity for the best performing model.

All four models were validated based on the area under the receiver operating characteristics curve (AUROC), the accuracy (sum of the true positive and the true negative rate), the error rate (opposite of accuracy) and the interquartile range (IQR) of the AUROC values in a non-spatial validation, i.e. data from all five key sites were used to train and test the models. These measures investigate the quality of the model, which is the ability to discriminate between bedrock and sediment locations. Test and training dataset have the same size and

replicate data points were preempted. The larger the AUROC the better is the model and thus the classification. A model classifying the data comparable to coincidence would have an AUROC of 0.5 and a model separating the classes perfectly of 1.0 (Sing et al., 2005; Fawcett, 2006; Hosmer et al., 2013). The AUROC was calculated using the ROCR package in R (Sing et al., 2005; r-project.org). The IQR is used as a measure of the transferability of the models (Petschko et al., 2014).

To validate and evaluate the classifier, we determined a probability threshold (cutoff value) using a compromise between sensitivity (true positive rate) and 1-specificity (false positive rate). This cutoff value was used to classify the modeled probabilities of bedrock/sediment occurrence of the best performing model into the classes bedrock and sediment. This model selected based on the highest median AUROC and mean accuracy values was applied to the whole area of the URB using the raster package in R (Hijmans, 2014; r-project.org). To test if the performance of the individual models (LR, PCLR, GAM) is significantly different, the Kruskal-Wallis rank sum and the Wilcoxon signed rank tests were used (overall and pairwise model comparison respectively, 5% significance level) (Hollander and Wolfe, 1999; Goetz et al., 2011).

Additionally, the results of the validation were used to estimate thematic consistency and variable importance. Thematic consistency shows the sensitivity of the model to sample variation. A high thematic consistency means a good quality and high robustness of the model. The importance of each variable is represented by the variable selection frequency calculated from the ten models fitted for the best performing model (Goetz et al., 2011; Petschko et al., 2014). It can be interpreted as a measure for the thematic consistency of the model (Guzzetti et al., 2006). A high thematic consistency is indicated by a variable selection frequency either close to 0% or close to 100%, which means the variable is never or always chosen.

Spatial transferability, i.e. spatial validation, was tested for a GAM2df (sample size: 51,200 pixels). The classifier was trained with 5 different input datasets, each consisting only of data points from four of the five key sites and then tested in the fifth, completely independent key site. Data from this site were not included when training the model. For each model the median AUROC and the IQR were estimated.

Furthermore, the impact of spatial heterogeneity within the study area and hence the input dataset in general on the model outcome were tested for a GAM2df (sample size: 20,000 pixels). The classifier was trained with six different input datasets, one comprised of data from all key sites and five only of data from one site. These six classifiers were tested in all key sites and in each single site, of which four are completely independent. For each model the median AUROC and the IQR were calculated.

### 3.4. Geomorphic analysis of modeled spatial distribution of sediment

The spatial distribution of sediment storages was further analyzed with the topographic position index (TPI) that is used to semi-automatically classify topographic slope position (TSP) and thus the position of the modeled sediment distribution:

$$TPI = z_0 - \bar{z} \quad (3)$$

where  $z_0$  is the elevation at the central point of the annulus and  $\bar{z}$  is the mean elevation of the annulus area (Guisan et al., 1999; Weiss, 2000). Positive TPI values indicate locations higher than the mean elevation of the surrounding area (e.g. hilltops and ridges), while negative TPI values are locations lower than the surroundings (e.g. valleys). TPI values around zero represent flat areas or locations with constant slope (Fig. 12). An outer and inner radius of 2000 and 1600 m of the annulus were chosen respectively to determine major landscape units (e.g. mountains, major ridge lines and major valleys). Six TSPs were classified based on the standard deviation of the TPI and the slope (Table 3) (Weiss, 2000). Based on this classification, the modeled

**Table 3**

Classification of topographic slope position (TSP) based on the topographic position index (TPI) after Weiss (2000). Sketch of TSP see Fig. 12.

Topographic slope position class	Threshold based on standard deviation (SD) of TPI	Slope [°]
Ridge and uppermost slope	>1 SD	
Upper slope	>0.5 SD, ≤1 SD	
(Middle) slope	>−0.5 SD, ≤0.5 SD	>10
Valley fill (main valley) and flat slopes	>−0.5 SD, ≤0.5 SD	≤10
Lower slope	≥−1 SD, ≤−0.5 SD	
Valley fills in tributaries	<−1 SD	

sediment distribution was further classified and the portion of sediment cover per class calculated.

## 4. Results

### 4.1. Model performance and comparison

Model comparison, i.e. non-spatial validation of LR, PCLR, GAM2df and GAM5df, reveals that the GAM5df achieves the highest AUROC values and thus the best results (Fig. 4). The PCLR yields the lowest accuracy and AUROC values, while the LR and GAM2df perform better. The median AUROC values of all four models, all between 0.8 and 0.9, indicate good performance and hence an excellent discrimination between sediment covered areas and bedrock areas (Hosmer et al., 2013).

The Kruskal-Wallis rank sum test, which compares the overall model outputs, shows significant differences between the AUROC and the accuracy values of the investigated models ( $p < 0.0001$ ). Furthermore, the pairwise comparison of the models using the Wilcoxon signed rank test also results in  $p$ -values  $< 0.0001$  for each test concerning the accuracy and the AUROC values. This indicates that significant differences exist between all four models, although the absolute differences in the median AUROC values and thus the quality of the models are small. However, the GAM5df performs significantly better than the other three models. IQR range between 0.0021 and 0.0025 and indicate good quality, high robustness and transferability of all models.

### 4.1.1. Influence of sample size on model performance

The selection and quality of predictive models is sensitive to different sample sizes, i.e. pixels, because the sample size has to be large enough to cover the variability of the predictor variables and to produce stable and reproducible results. However, the sample size should not be too large because it is probable to neglect the assumption of independent observations due to spatial autocorrelation and overparametrization, overfitting might arise (Heckmann et al., 2014) and computation times become very long. Therefore, we analyzed the sample size for the models using equal number of cases and controls ( $N = 100, 200, 400, 800, 1600, 3200, 6400, 12,800, 25,600, 51,200$ ). The quality of the models (i.e. the ability to discriminate between bedrock and sediment locations) and its stability was analyzed based on the effect of sample size reduction on the AUROC and the IQR. Moreover, the thematic consistency of the GAM2df was investigated for all sample sizes (Goetz et al., 2011; Petschko et al., 2014).

The sample size analysis shows similar results for all three models tested (PCLR, LR, GAM2df, Fig. 5). The PCLR returns stable AUROC values (median 0.8269) and narrow IQR (0.0020) with a sample size of only 6400 pixels that only slightly improve towards larger sample sizes. The LR also reaches relatively stable AUROC values (median 0.8374) with a sample size of 6400 pixels, but the IQR still declines from 0.0068 to 0.0023 (sample size 51,200 pixels) indicating a better transferability of the model. The GAM2df needs larger sample sizes of 51,200 pixels to reach a similar plateau with AUROC values increasing from 0.8607 to 0.8648 for sample sizes of 6400 to 51,200 pixels. This is probably associated with the model setup that is more data driven than the LR and the PCLR, which only model linear correlations between the dependent and the independent variables. The generally high AUROC values indicate a good quality of the model. A low IQR of 0.0021 for the GAM2df implies a good transferability of the model. However, the results of the GAM2df are better than the results of the other two models likewise for smaller sample sizes and thus a GAM should be the preferential model even if only a smaller dataset is available. Based on these results, a sample size of 51,200 pixels was chosen for each modeling approach achieving a better comparability. Furthermore, the thematic consistency, which was only investigated for the GAM2df (i.e. best performing model in sample size analysis), improves substantially with an increase of the sample size (see Supplementary material C). The total variable selection frequency in the GAM increases to 100% for most independent variables at a sample size of 51,200 pixels, thus the ten models built are very similar and the thematic consistency of the GAM model is high. Only two input variables, mean slope of the contributing area (ACCSLP) and profile curvature (10 m resolution, prc10), have a variable selection frequency of 50% and 60% respectively signifying a low thematic consistency, thus their relevance in the model is interpreted as relatively low. On the other hand, slope gradient (calculated from resampled 25 m DEM) yields a high variable selection frequency (100%) at a sample size of 400 pixels indicating a high importance of this variable in the model as well as the relevance of slope gradient for sediment erosion, transport and deposition.

### 4.1.2. Model performance of generalized additive model

The GAM5df (sample size: 51,200 pixels) as the best performing model is further analyzed and spatial prediction realized for the whole URB. The validation of the GAM5df shows an excellent performance (Hosmer et al., 2013) and a high transferability (median AUROC: 0.8739, IQR: 0.0022; Fig. 4). The thematic consistency of all but three variables (i.e. ACCSLP, plc10, prc10) is very high indicated by a total variable selection frequency of 100%. This means all ten independent and individually created models are very similar and comprise mostly the same input variables (Table 4). Most variables are chosen in every model run with a high number of degrees of freedom, thus the relation between the dependent and the independent variables is clearly non-linear.

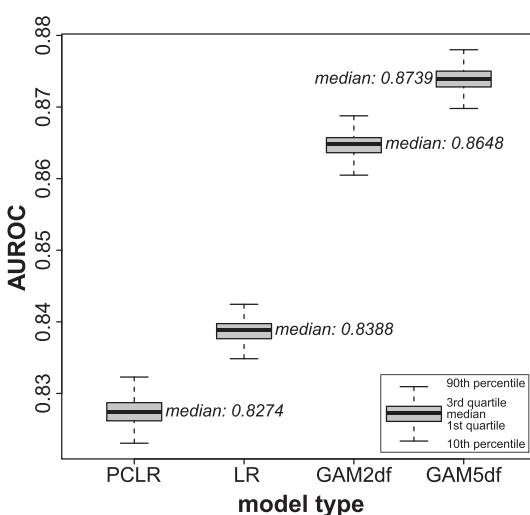


**Fig. 4.** Boxplots of area under the receiver operating characteristics curve (AUROC) values for all four applied models (sample size for all models 51,200 pixels, equal number of cases and controls): principal components logistic regression model (PCLR), logistic regression model (LR) and generalized additive model (GAM) with input variables transformed with a smoothing spline with two and five degrees of freedom respectively. AUROC values are derived from 25 fold non-spatial validation analysis performed ten times for each model (i.e. 250 values).

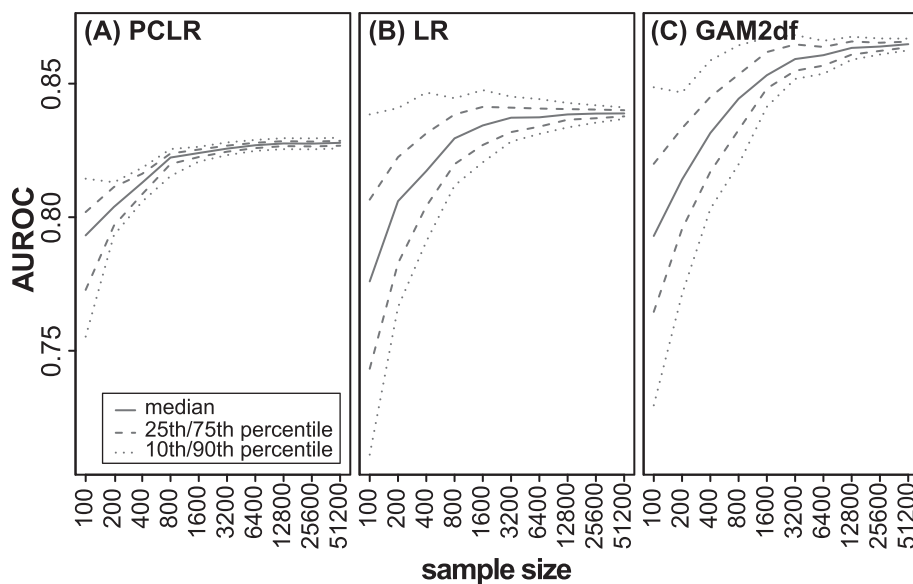


**Fig. 5.** Median, 10th, 25th, 75th and 90th percentile of AUROC (area under the receiver operating characteristics curve) values derived from ten times 25-fold validation of (A) the principal components logistic regression model (PCLR), (B) the logistic regression model (LR) and (C) the generalized additive model (GAM2df) for different sample sizes, i.e. number of pixels (equal number of cases and controls).

One of the ten independent and individually created models was applied to the URB due to the high thematic consistency and the high transferability of the models. The mean accuracy is  $78.35 \pm 0.18\%$ , which means on average 78.35% of all pixels are correctly classified based on cutoff values ranging between 0.4403 and 0.5109. A mean cutoff value of 0.4768 was chosen for the application of the model to the whole URB. The mean AUROC is  $0.8721 \pm 0.0012$ . Further measures illustrating the quality of the model are listed in Table 5.

#### 4.2. Modeled spatial sediment distribution

The model was applied to all areas of the URB (total area  $5382.3 \text{ km}^2$ ) that are not covered by glaciers or lakes (Bowles and Cowgill, 2012). The current glacier extent comprise an area of  $569.8 \text{ km}^2$  of the URB (Fischer, 2013) corresponding to 10.6%, while lakes only cover  $34.2 \text{ km}^2$  or 0.6%. Of the remaining  $4778.3 \text{ km}^2$  sediment covers  $2876.9 \pm 622.8 \text{ km}^2$  (53% of the URB) and bedrock

comprises  $1901.4 \pm 411.6 \text{ km}^2$  (35%) (Table 6). A visual comparison of the mapped sediment and bedrock distribution and the modeled sediment and bedrock classification in the five key sites shows good accordance (exemplary for the Minstigertal, Goms; Fig. 6). The overall spatial distribution of sediment in the URB shows a high degree of variability at different scales. However, the basic pattern of sediment-filled valley floors and bedrock in the location of peaks and the highest elevations is apparent. The valley fill of the Upper Rhone Valley is also correctly classified as sediment, while bedrock is exposed on the very steep sides of the U-shaped valley.

The spatial variability of the modeled sediment coverage in the URB was additionally analyzed by calculating the relative sediment cover in watersheds on different spatial scales (Fig. 7). The considered watersheds are characterized by glacier and lake coverage of <50% and a valley fill cover of <40% (Bowles and Cowgill, 2012; Blöthe and Korup, 2013; Fischer, 2013). At small spatial scales (<5  $\text{km}^2$ ), areal sediment cover varies between 0 and 100%. However, no clear pattern is apparent,

**Table 4**

Thematic consistency of generalized additive model with input variables transformed with a smoothing spline with five degrees of freedom (GAM5df) based on ten individual models build. Relative variable selection frequencies as well as the variable selection frequencies of non-transformed (N) and transformed (S) variables are calculated for each independent input variable.

	Variable selection frequency [%]	Non-transformed	Transformed (2df)	Transformed (3df)	Transformed (4df)	Transformed (5df)
ACCLOG	100	–	1	–	2	7
ACCSLP	40	–	–	–	–	4
ASP_EW	100	–	–	–	–	10
ASP_NS	100	–	6	2	2	–
DEM	100	–	–	–	–	10
HI40	100	–	–	–	–	10
NDR	100	–	–	–	–	10
NDVI	100	–	–	–	–	10
PLC10	70	–	–	–	–	7
PLC25	100	–	–	–	–	10
PRC10	50	–	–	5	–	–
PRC25	100	–	–	–	–	10
ROU	100	–	–	–	–	10
ROU25	100	–	–	–	–	10
SLP	100	–	–	–	–	10
SLP25	100	–	–	–	–	10
SR	100	–	–	–	–	10
VDC	100	–	–	–	–	10

**Table 5**

Evaluation and confusion matrix of generalized additive model with input variables transformed with a smoothing spline with five degrees of freedom (GAM5df) based on 25-fold validation (AUROC = area under the receiver operating characteristics curve, SD = standard deviation, TPR = true positive rate, TNR = true negative rate, TP = true positives, FP = false positives, FN = false negatives, TN = true negatives).

Mean AUROC ± 1SD	0.8721 ± 0.0012
Mean accuracy ± 1SD [%]	78.3519 ± 0.1838
Range of cutoff values	0.4403–0.5109
Mean cutoff value ± 1SD	0.4768 ± 0.0156
Mean odds ratio ± 1SD	13.2769 ± 0.2876
TPR/sensitivity ± 1SD [%]	76.1375 ± 1.3600
TNR/specificity ± 1SD [%]	80.5663 ± 1.2783
Confusion matrix	
	Predicted bedrock cover (1)
	Predicted sediment cover (0)
Actual bedrock cover (1)	TP: 0.3807 ± 0.0068
Actual sediment cover (0)	FP: 0.0972 ± 0.0064
	FN: 0.1193 ± 0.0068
	TN: 0.4028 ± 0.0063

and watersheds with high sediment coverage are often located next to those with low sediment coverage (Fig. 7). With increasing spatial scale (5–100 km<sup>2</sup>), and a decreasing absolute number of watersheds in the respective class, overall variability decreases and peaks for bedrock and sediment coverage become more pronounced, with highest densities for bedrock (30–40%) being consistently lower than for sediment cover (60–65%) (Fig. 7).

## 5. Discussion

### 5.1. Predictive modeling of spatial sediment distribution

Predictive models have been applied in a variety of geomorphological studies including landslide hazard analysis (Petschko et al., 2014; Goetz et al., 2015), the spatial distribution of permafrost landforms (Brenning, 2009), geomorphological mapping (Luoto and Hjort, 2005), and the spatial variability of soil organic carbon stocks (Hoffmann et al., 2014). In the present study, we used predictive modeling to distinguish between sediment and bedrock and, judging from the AUROC values, all applied models showed satisfying results (Fig. 4), though differences of the models' quality are significant. Moreover, model robustness and transferability, both crucial model properties when modeling natural phenomena, are high, as indicated by the low IQR. However, small differences between the performance of different statistical and machine learning models is not exceptional (e.g. Luoto and Hjort, 2005; Marmion et al., 2008; Goetz et al., 2011; Goetz et al., 2015), thus model evaluation should not solely be based on the estimated error rate or other quantitative performance measures such as AUROC (Steger et al., 2015). Instead, other qualitative and quantitative measures more in line with research questions and aims should be included

in model evaluation and selection (Luoto and Hjort, 2005; Goetz et al., 2015; Steger et al., 2016). These measures include for example the geomorphic plausibility of a predictive map, which means the results should demonstrate no bias related to input data, show no algorithm artifacts, and have high AUROC values (Steger et al., 2016). We thus focus on several configurations that are important for our aims, e.g. the spatial and non-spatial validation, influence of input parameters, sample size, robustness of model, and variable importance.

The three different models applied were chosen due to their good interpretability (Goetz et al., 2011; Goetz et al., 2015), their wide application in geomorphic research and reliable results in earlier studies. Besides, machine learning techniques, such as random forest or support vector machine, are more prone to overfitting, difficult to interpret ("black boxes") and produce a rather noisy and heterogeneous prediction surface (Brenning, 2005; Goetz et al., 2015; Steger et al., 2016). Generalized linear and generalized additive models are continuous functions of the predictors (Formulas (1), (2)), thus they produce smooth and visually appealing prediction surfaces, i.e. prediction maps without single pixels classified incorrectly in an otherwise heterogeneous area and without artifacts from the algorithm (Fig. 6). This is of high importance, as our aim is to deliver a geomorphic interpretation of the spatial distribution of sediments. Based on the median AUROC the best performance (0.8739) was obtained with the GAM5df (Fig. 4), which is in good agreement with other studies (e.g. Marmion et al., 2008; Brenning, 2009; Petschko et al., 2014; Goetz et al., 2015).

#### 5.1.1. Spatial validation and heterogeneity within a large scale drainage basin

Besides the non-spatial validation (Fig. 4), we apply a spatial validation procedure by training and testing five models with different input datasets. Training datasets were taken from four of the five key sites. This model is tested and errors are estimated in the fifth key site. The datasets from the five key sites are assumed to be completely independent as they are far enough apart to avoid spatial autocorrelation (Brenning, 2005; Brenning, 2012) and exhibit differing characteristics (Fig. 1, Table 1). This allows us to check how the model performs in areas where no sampling took place (Fig. 8). In contrast, the commonly used approach to select a model is a non-spatial validation performed by splitting the dataset into training and test datasets (often without repeated or cross-validations). This approach has considerable drawbacks due to the dependence of training and test data (Brenning, 2005): it produces results too overoptimistic, underestimates error rates, causes overfitting, and does not allow an estimation of the model robustness because only one error rate or AUROC can be estimated especially when applying flexible machine learning methods.

Overall, the results of the non-spatial validation (Fig. 4) are better than of the spatial validation (Fig. 8). However, the performance estimates from the spatial validation are more realistic and do not overestimate the ability of the predictor (Brenning, 2005; Petschko et al., 2014). In the Val d'Illiez and the Turtmannal, the models perform better than the GAM2df, trained and tested in all key sites (Fig. 4). The models in the Goms and the Lötschental perform only slightly poorer. However, the results of the spatial validation in the Val de la Liène are strikingly low. In the four key sites where the spatial validation yields median AUROC values above 0.8, the IQR are very low (0.0019–0.0028), indicating high model robustness and transferability, which is also lower in the Val de la Liène (0.0160). These results suggest that further investigation of the differing site conditions in the key sites and the heterogeneity within the URB is necessary (Table 1).

The poor performance of the GAM2df for the Val de la Liène using a spatial validation can be associated with a variety of factors, including lithology, erodibility, topography, and glacial imprint. The Val de la Liène features mostly Mesozoic limestones of the Helvetic sedimentary nappes distinguished by a medium erodibility (Kühni and Pfiffner, 2001) and is situated north of the Rhone Valley. It is located at lower elevations, where contemporary glacial extent is low (c. 1.2%) (Fischer,

**Table 6**

Modeled surface extent of bedrock and sediment within the Upper Rhone Basin based on generalized additive model (GAM) with smoothing spline transformation of input variables and up to five degrees of freedom. Results were classified based on an optimal compromise between sensitivity and 1-specificity of the predicted probabilities. Glacier extent from Swiss glacier inventory 2010 (Fischer, 2013). Lakes classified based on digital elevation model (DEM) with a semi-automated surface classification model (Bowles and Cowgill, 2012).

Class	Modeled surface extent [km <sup>2</sup> ]	Modeled surface extent [%]
Sediment	2876.93 ± 622.80	53.45 ± 21.65
Bedrock	1901.37 ± 411.61	35.33 ± 21.65
Glacier (data from Fischer, 2013)	569.78	10.59
Lakes (based on SCM algorithm by Bowles and Cowgill, 2012)	34.22	0.64
Total area	5382.30	100.00

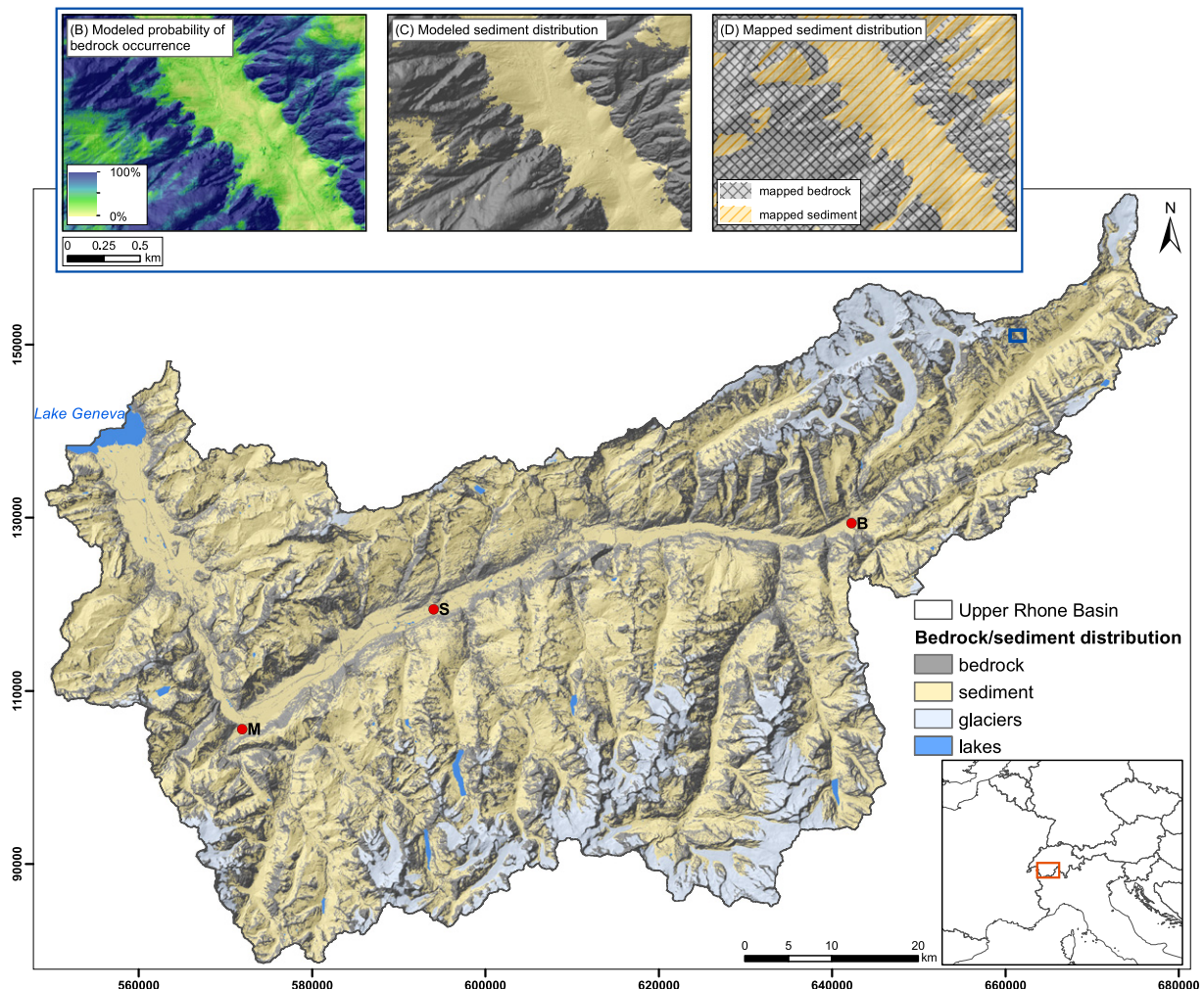


**Fig. 6.** (A) Modeled bedrock and sediment distribution within the Upper Rhone Basin (M = Martigny, S = Sion, B = Brig) based on generalized additive model (GAM) with smoothing spline transformation of input variables and up to five degrees of freedom. Results were classified based on an optimal compromise between sensitivity and 1-specificity of the predicted probabilities. Glacier extent from Swiss glacier inventory 2010 (Fischer, 2013). Lakes classified based on digital elevation model (DEM) with a semi-automated surface classification model (Bowles and Cowgill, 2012). (DEM from swissstopo, projection: CH1903). Insets show (B) modeled probability of bedrock occurrence, (C) modeled bedrock and sediment distribution and (D) mapped bedrock and sediment distribution in detail for the Minstegital, Goms.

2013). Pleistocene glacial imprint is less pronounced due to the absence of an ice dome in this region (Kelly et al., 2004), the asymmetry of the URB with smaller tributaries in the north, the lower elevations and thus the formation of a major valley glacier. These site conditions distinguish the Val de la Liène strongly from the Goms, the Turtmanntal and the Lötschental. The Val d'Illiez, however, located in the westernmost part of the URB where the Rhone Valley is oriented in a NNW direction, has some conditions in common. It is dominated by the Infrahelvetic nappes and the South- and Ultrahelvetic sedimentary nappes consisting dominantly of flysch, and Mesozoic and Tertiary limestone with a low to medium erodibility (Kühni and Pfiffner, 2001). Only the NW part is underlain by the non-metamorphic Prealps (detached Upper and Middle Penninic nappes). The Val d'Illiez is also located at relatively low elevations, resulting in only minor glacial extent today (c. 1.2%). Albeit, the Val d'Illiez is characterized by a distinct glacial topography left behind by Pleistocene valley glaciers flowing from the SW (Kelly et al., 2004). The remaining three key sites have a higher contemporary glacial extent (10.8–14.2%), are dominated by lithologies with a low erodibility (metamorphic and plutonic rocks) and are located at higher elevations (Table 1). These lithological differences find their expression in the chemical denudation that is responsible for one third of total denudation in the sedimentary units of the Alps as opposed to only 10% in regions dominated by crystalline rocks (Hinderer et al., 2013). Hence,

lithology might set upper boundaries to storage of clastic sediment. Besides lithology, differing Pleistocene glacial imprint seems to have an influence on the performance of the model in the URB. Schlunegger and Norton (2013) concluded the inheritance of Pleistocene glaciations have the strongest influence on current erosional forces and the landscape in the Central Alps and thus possibly on the spatial distribution of sediment. Future studies should further investigate these and other influential factors with heterogeneous distribution within a large scale area, e.g. current uplift rates (Kahle et al., 1997; Schlatter et al., 2005) and long-term exhumation ages (Vernon et al., 2008).

#### 5.1.2. Influence of data input and potential sources of error

Analysis of the influence of the input dataset on the performance of the model (Fig. 9) show that models trained with data from all key sites perform best when tested in all key sites (median AUROC = 0.8655). However, these models do not perform as good in the single key sites with median AUROC values ranging between 0.7454 in the Val d'Illiez and 0.8385 in the Turtmanntal (Fig. 9). If only one site would have been sampled for model training purposes, the performance in the remaining URB would be less good. Not surprisingly, the highest median AUROC values are obtained when a model is trained and validated with data from only one key site. These key sites are on the one hand characterized by a low heterogeneity, on the other hand training and

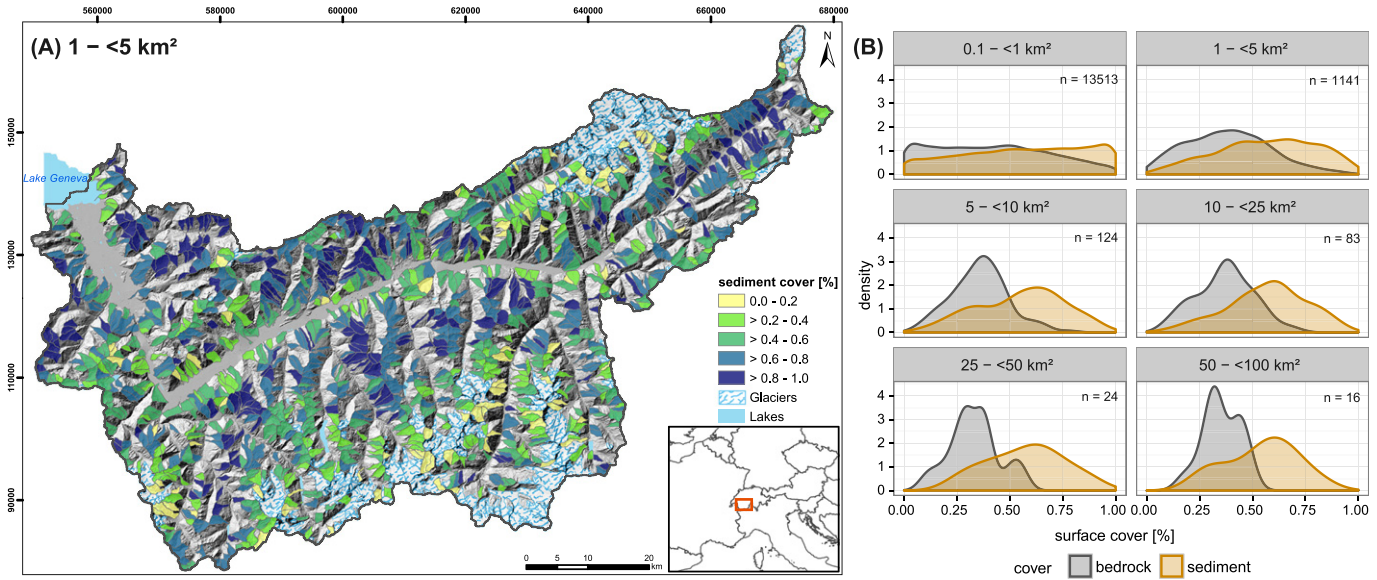


**Fig. 7.** (A) Map of the spatial variability of the modeled sediment cover [%] in watersheds with a spatial scale of  $1- < 5 \text{ km}^2$  in the Upper Rhone Basin. Glacier extent from Swiss glacier inventory 2010 (Fischer, 2013). Lakes classified based on digital elevation model (DEM) with a semi-automated surface classification model (Bowles and Cowgill, 2012) (DEM from swisstopo, projection: CH1903). (B) Probability density functions show the density [%] of modeled sediment and bedrock cover for each spatial scale of watersheds ( $0.1- < 1 \text{ km}^2$ ,  $1- < 5 \text{ km}^2$ ,  $5- < 10 \text{ km}^2$ ,  $10- < 25 \text{ km}^2$ ,  $25- < 50 \text{ km}^2$ ,  $50- < 100 \text{ km}^2$ ).

testing dataset are presumably not independent due to spatial autocorrelations (Brenning, 2005). Again, we point out site conditions in the Val de la Liène must be distinctly different from the other sites since models trained with data from this site perform weakly in the other four key sites.

Both results (Figs. 8, 9) indicate the importance of local site conditions, which has been pointed out in previous studies (Blahut et al., 2010; Petschko et al., 2014). As overall topographic and morphological characteristics do not vary notably throughout the URB (Table 1), we decided to train one model for the whole URB with one large input

dataset from all five key sites representing the heterogeneity, instead of training individual models for homogeneous regions (Petschko et al., 2012). This attempt yields good results in the URB. Training several models produces problems such as subjective subdivision, more data input, and more model training validation and application runs with longer computation times. Our results highlight the importance of a sensible selection of key sites and thus the sampling design, which are both vital for the model performance. Spatial transferability can only be achieved when the input dataset reflects the properties and heterogeneity of the region.

Based on the sample size analysis (chapter 4.1.1) and quality assessment of the applied model, we infer that a minimum sample size of at least 25,600 pixels ( $2 \times 2$  m resolution) of sediment cover and bedrock each needs to be mapped to set up a robust GAM. This would be

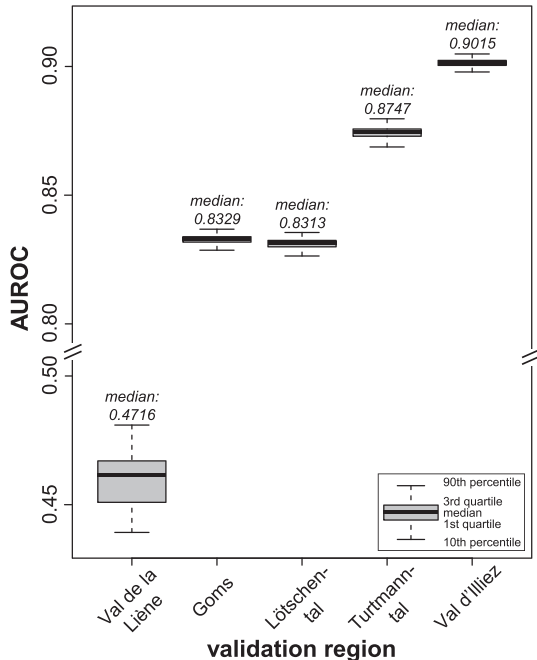


**Fig. 8.** Spatial validation: training datasets consist of data from four of the five key sites and the model, a generalized additive model with input variables transformed with a smoothing spline with two degrees of freedom (GAM5df), is then tested and AUROC values are estimated in the fifth site (sample size for all models 51,200, equal number of cases and controls). AUROC values are derived from ten times 25 fold validation.

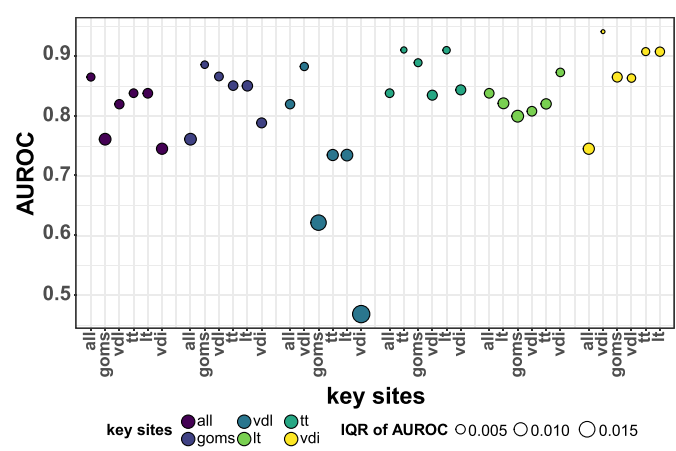


**Fig. 9.** Spatial heterogeneity and spatial transferability of generalized additive model with smoothing spline transformation of input variables and up to two degrees of freedom (GAM5df). Models were trained with data from all and each single key site and then tested in all sites and each single site. Testing consists of applying ten times a 25-fold validation. Sample size for all training and testing datasets is 20,000 (equal number of cases and controls). Color of bubbles indicates the spatial origin of the input data for model training. AUROC values signify the quality of the models. Bubble size represents the IQR (interquartile range of the AUROC) values, which are used as a measure of the transferability of the models. (all = all key sites, vdl = Val de la Liène, goms = Goms, lt = Lötschental, tt = Turtmannal, vdi = Val d'Illiez).

equivalent to an area of c. 0.2 km<sup>2</sup> distributed across the five key sites with the pixels spread far apart to minimize spatial autocorrelation. However, this only includes setting up one model without validation, i.e. ten times a 25-fold validation in this study corresponds to 10.7 km<sup>2</sup> of mapped area. Moreover, the samples need to capture not only the spatial heterogeneity within the URB represented by the five key sites but also several characteristics within the key sites, e.g. different spatial scales, elevations, slope gradients and topographic slope positions as well as the possibly occurring sediment storage types. Further spatial validation in this study required a total of 2.1 km<sup>2</sup> of sediment cover and bedrock each mapped in every key site, summing up to 20.8 km<sup>2</sup> in the URB. Even though a relatively small area of 20.8 km<sup>2</sup> (c. 0.4% of the URB) could be sufficient to achieve the presented modeling results, the pixels would have to be spread out relatively even across the five key sites and a point-based mapping would be much more time consuming than an area-covering mapping approach. Based on our results, we can recommend for future studies to map the spatial distribution of a geomorphic feature, e.g. sediment distribution, in different key sites representing the heterogeneity of the whole study area and to map an area spread out evenly and representing the relevant system characteristics. Nevertheless, a smaller area than the mapped 6.7% of the URB, i.e. 360.3 km<sup>2</sup> (Table 1), should be sufficient to model the spatial sediment distribution of a large scale drainage basin.

Besides the error rate of the applied model (Table 5, 21.7% for the GAM5df), other errors are more difficult to quantify. First, errors arise during mapping of sediment storages in the five key sites and due to uncertainties in the digital elevation model, which is the basis for most of the predictors. Furthermore, only areas presently free of glacial ice can be modeled (c. 90% of URB), as the underlying material (sediment/bedrock) of glaciers cannot be analyzed. We assume that the five key sites represent the heterogeneity of the URB and that the predictive model performs well in both sampled and not sampled sites. However, error quantification with validation procedures is not possible in regions which were not considered by field mapping. Even though the selected candidate predictors incorporate a large variety of processes influencing the distribution of sediment, we cannot rule out the possibility to have missed out influencing factors.

## 5.2. Geomorphic implications of modeled sediment distribution

Slope gradient, as one of the key factors driving sediment erosion, transport and deposition and thus sediment cover, constitutes an important variable in the applied models (Chapter 4.1.1). Hence, it was used to compare the mapped and modeled spatial distribution of sediment cover in the five key sites (Fig. 10). While the prediction performs well with an accuracy of c. 78% and displays the overall pattern of sediment distribution correctly, relative sediment cover in areas with slope gradients <30° tends to be overestimated by the applied model in comparison to the field mapping results. This is especially the case in limestone dominated, deglaciated areas located in the north of the URB, where other erosional processes, i.e. carbon dissolution, might cause a difference in surface morphology. Furthermore, very flat bedrock-dominated glacier forefields are affected by misclassification. Sediment coverage is slightly underestimated in areas with slope gradients >50°. These are often the ridges of steep side moraines. Apart from these special situations, even steep sediment storage types, i.e. talus and sediment-filled couloirs, were correctly classified and precisely delineated from the bordering bedrock.

### 5.2.1. Sediment storage variability in the Upper Rhone Basin

Several factors potentially govern the spatial distribution of sediment storages and the great spatial variability of sediment cover, i.e. topography, connectivity, glacial imprint, lithology and tectonic uplift (Chapter 5.1.2). Headwaters in the URB feature a very strong variability of sediment coverage (Fig. 7). Watersheds with a high degree of sediment cover are located right next to watersheds with minor sediment

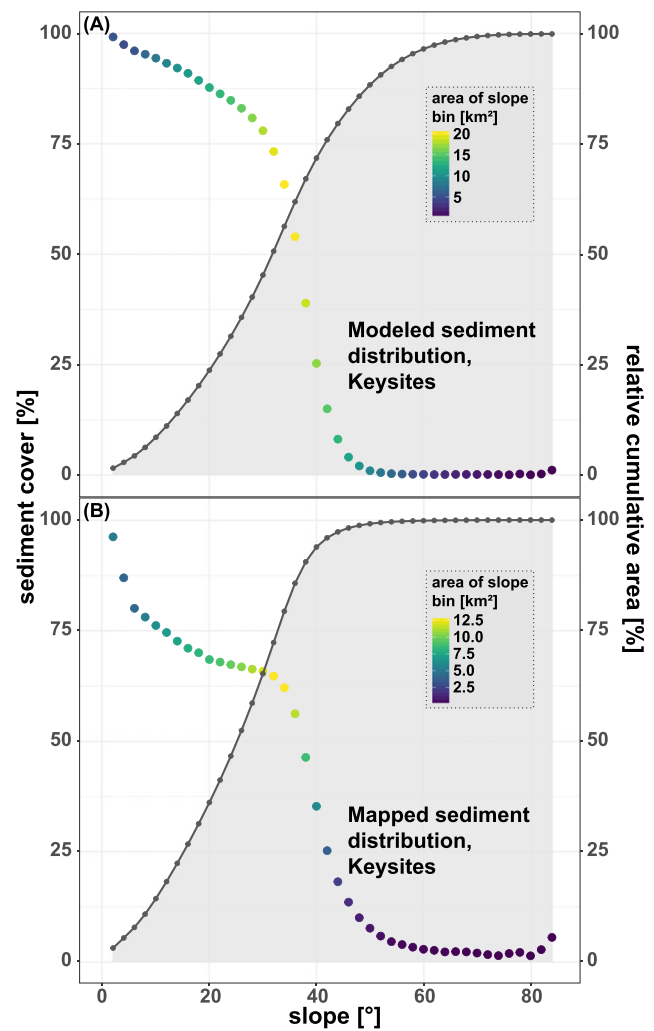


**Fig. 10.** Sediment cover [%] as a function of slope (points) in the five key sites based on (A) the modeled and (B) the mapped sediment distribution. Points are color-coded by total area of each elevation bin. The cumulative sediment coverage is given by the gray line.

coverage, i.e. it ranges from 0 to 100% in watersheds <5 km<sup>2</sup>. Previous studies investigating sediment storage in alpine catchments focus on one or several catchments (usually 10<sup>0</sup> to 10<sup>2</sup> km<sup>2</sup>). In the Turtmannalp 75% of the hanging valleys are covered with sediment (Otto et al., 2009), whereas this portion is only 34% of Val Müschauns, located in the easternmost part of Switzerland (Messenzehl et al., 2014). In the Canadian Rocky Mountains sediment coverage in five catchments ranges between 44% and 82% (Hoffmann et al., 2013). However, the actual variability of sediment cover in headwaters in a large scale drainage basin, i.e. the URB, is much greater.

In general, relative sediment cover decreases with increasing elevations in the URB (Fig. 11). Sediment cover as well as volume (e.g. Hinderer, 2001; Mey et al., 2015) is highest in elevations up to 500 m (80–92%) representing the valley fill of the Rhone Valley up to Sion. At elevations between 500 and 700 m the relative sediment cover is strongly reduced (52%), although this bin comprises mostly the valley fill of the Rhone Valley up to Brig but also partly the trough walls and the incised bedrock gorges of the tributaries of the lowermost URB, both featuring low sediment cover. Despite the general decreasing trend of sediment cover with rising height, the relative sediment cover increases steadily from 37 to 65% at elevations from 700 to 1300 m. These elevations represent the transition zones from the Rhone Valley to the tributaries, which are characterized by low

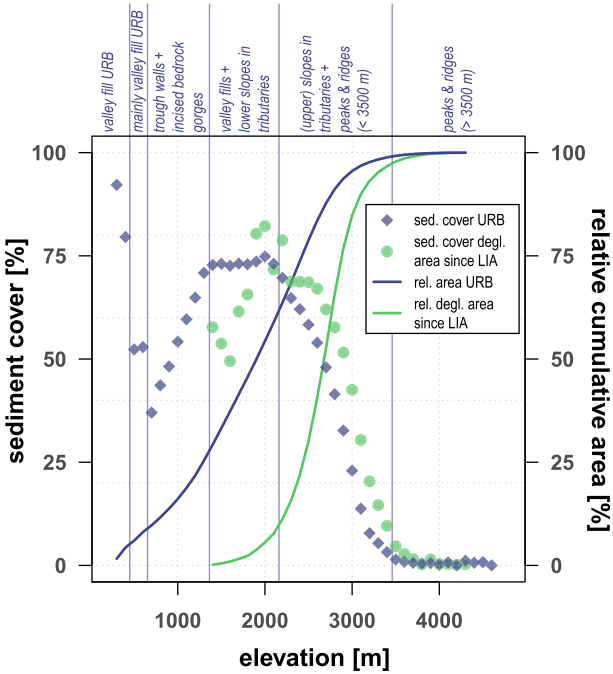


**Fig. 11.** Sediment cover [%] as a function of elevation for the Upper Rhone Basin (blue diamonds) and the deglaciated area since the Little Ice Age (green dots). The area was stratified into 100 m-elevation bins (for location of bins see map in Supplementary material D). The cumulative sediment coverage is given by the lines (blue = Upper Rhone Basin, green = deglaciated area). Deglaciated area since the Little Ice Age was delineated based on datasets by Maisch (2000) and Fischer (2013).

sediment coverage and storage (Fig. 6, Fig. 11) due to steep gradients, V-shaped valleys or gorges (e.g. Schlunegger and Hinderer, 2003; Norton et al., 2010; Valla et al., 2010a; Valla et al., 2010b). River incision and retreating knickpoints will continuously lower the valley floors and increase the connectivity to the channel and the catchment outlet.

Currently, lots of sediment is stored further up in the tributaries above knickpoints. More than two thirds (70–73%) of the valley floors and lower slopes are covered with sediment due to the so far weak re-mobilization, the low sediment connectivity between hillslopes and channels and low transport capacities along channels of the now ice-free, wide, U-shaped and flat cirque floors (e.g. Schrott et al., 2003; Brardinoni and Hassan, 2006; Otto et al., 2009; Götz et al., 2013; Hoffmann et al., 2013). The upper slopes, peaks and ridges show a decreasing sediment cover with increasing elevation and the highest peaks and ridges ( $> 3500$  m) are basically free of sediment. This points to the relevance of sediment cover and thus storage in the valley fills and at lower slopes of the tributaries of large scale drainage basins.

Based on an investigation of 57 headwaters, Hoffmann et al. (2013) concluded that erosion rates are higher in headwaters with distinct cirque morphology and yet the sediment delivery ratios are lower resulting in higher sediment storage. This pattern of sediment distribution is featured in the tributaries of the URB. It shows that the landscape and thus the low sediment connectivity and the sediment distribution in the URB are strongly inherited by the Pleistocene glacial imprint. However, fluvial and other post-glacial processes progressively reshape the alpine environment. Thus, the landscape is in a transient state adjusting to fluvial conditions (Brunsden and Thornes, 1979; Ballantyne, 2002; Brardinoni and Hassan, 2006; Schlunegger and Norton, 2013; Hoffmann, 2015). Further studies should focus on the transition zones and their role in sediment dynamics (e.g. Valla et al., 2010a; Van den Berg et al., 2012) and especially in the reworking of sediment storages. If sediment delivery ratios to the main valley increase, large amounts of sediment will potentially be mobilized, which might

be a hazard in the future. However, the glacial imprint in the hanging valleys limiting sediment fluxes may persist until the onset of the next glaciation (Brardinoni and Hassan, 2006; Hoffmann, 2015), since fluvial adjustment of the transition zones is rather slow with incision rates on the order of several  $\text{mm a}^{-1}$  (e.g. Korup and Schlunegger, 2007; Valla et al., 2010a). Hoffmann (2015) demonstrates that paraglacial response times of sediment flux in mountain headwaters in the Canadian Rocky Mountains range in the order of 100–400 ka. Thus, the sediments stored above knickpoints will probably remain there for a long period of time.

### 5.2.2. Sediment cover in different topographic positions

For a more detailed analysis of the modeled spatial distribution of sediment storage in the URB, the areas covered with sediment were further classified according to six TSP (Weiss, 2000) (Fig. 12) indicating the importance of different sediment storage types, which are typical for certain topographic positions. Excluding glaciated areas, sediments cover c. 60% of the URB. The broad valley of the Upper Rhone alone accounts for c. 9% of this area ( $260 \text{ km}^2$ , 4.8% of URB) (Mey et al., 2015), leaving  $> 90\%$  covered with other types of sediment storage (Table 7). These sediment storages outside the trunk valleys have often been neglected in large scale sediment budgets.

The ridges, upper and middle slopes constitute c. 55% of all sediment coverage, translating to 25% of the whole area of the URB. Despite their limited thickness ( $10^{-1}$  to  $10^1 \text{ m}$ ), Hoffmann et al. (2013) found these diffusive hillslope storages play a significant role in the sediment budgets of large scale alpine drainage basins. This is supported by other studies, where diffusive hillslope storages range between 25 and 35% of the sediment covered area (Otto et al., 2009; Messenlehrl et al., 2014).

Sediments at the lower slopes and fringing the thalwegs of tributaries comprise c. 28% of sediment coverage in the URB. These sediments are deposited mainly by rock falls, debris flows and fluvial processes at locations with low slope gradients and transport capacity and their storages have greater thicknesses. Otto et al. (2009) lists depths up to 23.5 m for talus deposits in mountain headwaters and Götz et al. (2013) investigated even greater thicknesses for debris flow cones in the Gradenmoos basin, Austria. Talus and debris flow deposits have been identified as major sediment storages in several small scale mountain catchments. In the Reintal 72% of the sediment covered area is dominated by talus and debris flow deposits (Schrott et al., 2003), in the Val Müschauns they account for almost 50% of the sediment covered area (Messenlehrl et al., 2014), and talus deposits cover 20% of a hanging valley in the Turtmannal (Otto et al., 2009). Although the relative areal extent of these storage forms is lower in large scale drainage basins, their role in large scale sediment budgets needs to be quantified (Sass, 2007). The last class comprises primarily the valley fill in the Upper Rhone Valley and fewer flat areas on slopes (total 12.4%). Some of the valley fills in the very large tributaries are also classified in this category. These two units cannot be further subdivided in this classification because of morphological similarities (Table 3). Glacial sediment storages, which constitute a significant portion in the hanging valleys of the Turtmannal (Otto et al., 2009), are difficult to identify based on the approach using topographic slope positions since they are not deposited in one typical position. However, the presented model on the spatial sediment distribution has great potential to build the basis for a detailed sediment budget in a large scale drainage basin investigating quantitatively the importance of small scale sediment storages in comparison to large valley fills, e.g. in the Upper Rhone Valley. Detailed large scale sediment budgets are still rare (e.g. Jäckli, 1957; Jordan and Slaymaker, 1991; Tunnicliffe and Church, 2011; Tunnicliffe et al., 2012), as approaches to bridge the gap between scales are difficult to establish.

Earlier studies on large scale sediment storage in the URB focused on the Rhone Valley itself, while not including storage in small headwater basins or in talus and slope deposits. Volumetric estimates of the sediments stored in the wide, glacially overdeepened valley between Brig and Lake Geneva (Fig. 1) range between 80 and 106  $\text{km}^3$  based on

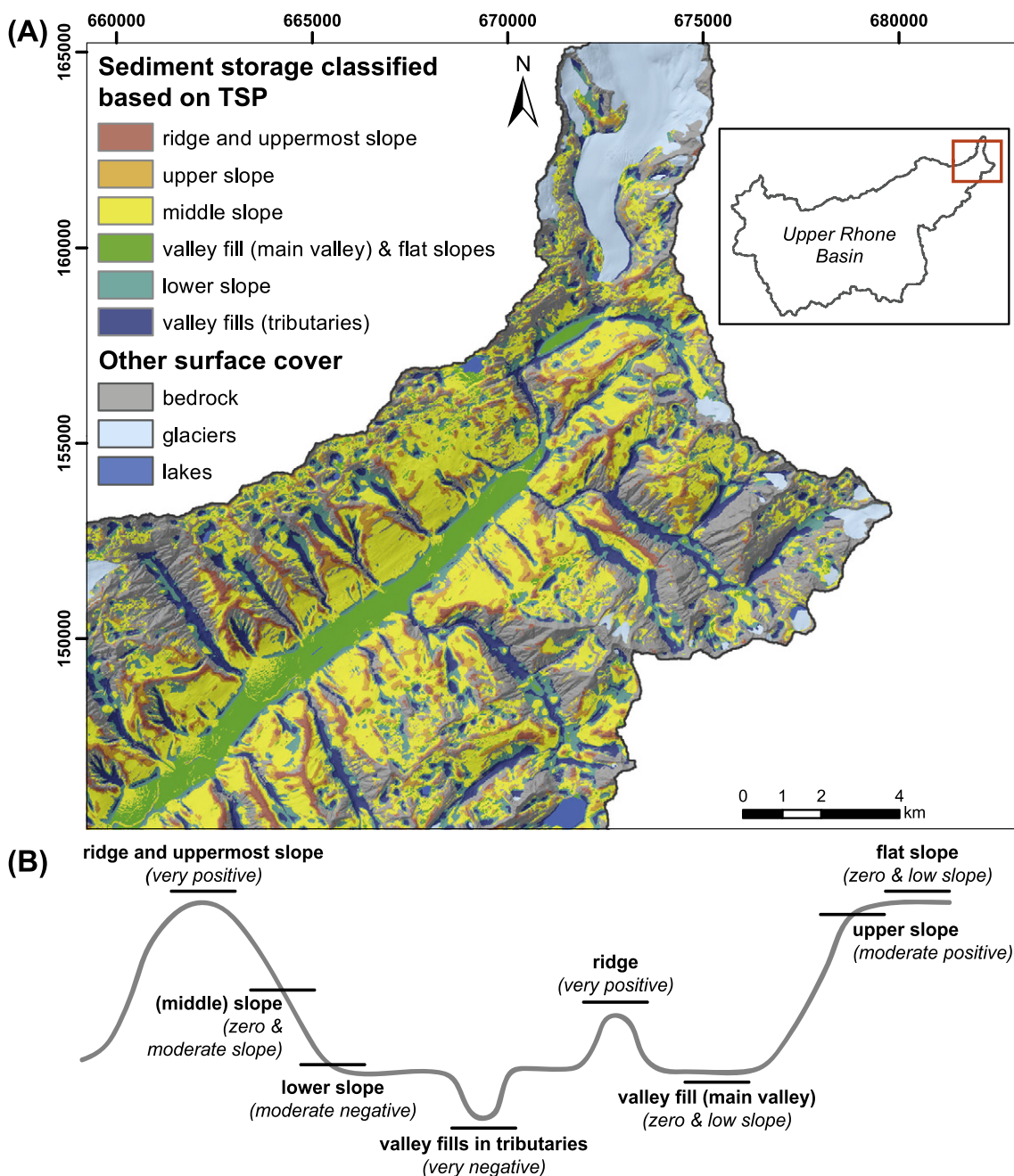


**Fig. 12.** (A) Modeled sediment distribution classified according to topographic slope position (TSP) based on the topographic position index (TPI) after Weiss (2000) in the Goms region, Upper Rhone Basin. Glacier extent from Swiss glacier inventory 2010 (Fischer, 2013). Lakes classified based on digital elevation model (DEM) with a semi-automated surface classification model (Bowles and Cowgill, 2012) (DEM from swisstopo, projection: CH1903). (B) Sketch of TSP and TPI and slope values after Weiss (2000).

different approaches (Hinderer, 2001; Rosselli and Olivier, 2003; Jabyedoff and Derron, 2005; Mey et al., 2015), with errors of up to  $\pm 50\%$  (Hinderer, 2001). Since the valley fill in the Rhone Valley accounts for 240 km<sup>2</sup> of the sediment coverage in the URB, the remaining c. 2600 km<sup>2</sup> must be covered with other sediment storages (Table 6). Conservatively assuming a mean depth of 1–5 m for these sediment storages, would translate to a volume of 2.6–13 km<sup>3</sup> (i.e. 2–16% of the sediment volume stored in the Rhone Valley between Brig and Lake Geneva), underscoring the significance of small scale sediment storages. We note that this is a very conservative estimate because sediment storages deposited at lower slopes or in thalweg positions in the tributaries, larger fans and valley fills have reportedly higher depth than 5 m (e.g. Schrott et al., 2003; Sass, 2006; Sass, 2007; Otto et al., 2009;

Götz et al., 2013; Hoffmann et al., 2013). Thus, realistic estimations considering spatial scale effects on sediment thickness would yield much higher sediment volumes in small scales sediment storages.

### 5.2.3. Sediment cover in deglaciated areas since the LIA

The rapid deglaciation in the European Alps since the Little Ice Age (Maisch, 2000; Zemp et al., 2008) and especially in the last decades (Haeblerli et al., 2007; Fischer et al., 2014) exposed large areas that were previously buried beneath ice. With ongoing glacial melt, this trend will continue within the next decades (Huss et al., 2017). Studies focusing on sediment storage in deglaciated areas on a larger scale are so far missing. Thus, we will contribute to this research gap by investigating the sediment cover in the areas deglaciated since the Little Ice

**Table 7**

Sediment storage [ $\text{km}^2$  and %] per topographic slope position (TSP) class based on the topographic position index (TPI) after Weiss (2000).

Topographic slope position (TSP)	Area [ $\text{km}^2$ ]	Area [%]
Ridge and uppermost slope	131.32	4.56
Upper slope	255.20	8.87
(Middle) slope	1328.01	46.16
Valley fill (main valley) and flat slopes	356.08	12.38
Lower slope	493.42	17.15
Valley fills (tributaries)	312.90	10.88
Total	2876.93	100

Age in a large scale catchment. In the URB an area of  $355.8 \text{ km}^2$  has been deglaciated since the LIA (Maisch, 2000; Fischer, 2013), of which  $201.4 \text{ km}^2$  (c. 56.6%) are covered with sediment,  $152.7 \text{ km}^2$  (42.9%) with bedrock and the remaining parts (0.5%) with lakes. This is similar to the areal extents of sediment and bedrock cover in the URB, with c. 60% of the non-glaciated area covered with sediment and c. 40% with bedrock. The exposed areas, largely located in the glacier forefields between 1900 and 3000 m, are mainly covered with unconsolidated, barely vegetated and thus unstable sediments (Baewert and Morche, 2014; Lane et al., 2017). But also smaller areas surrounding the upper parts of glaciers will be deglaciated, where bedrock is exposed due to glacial thinning (Fig. 11). These areas located above 3500 m amount to only 5% of the total deglaciated area and the sediment cover is <10%. The sediment coverage is characterized by a general decrease with increasing elevation in the deglaciated areas (Fig. 11), a trend that also holds for the whole URB. However, in direct comparison to areas without recent glacial imprint, the relative sediment cover in the deglaciated areas is distinctly higher (up to 82%) at elevations ranging from 1900 to 3500 m. Deglaciated areas below 1900 m (cumulative area 2.5%) show a large scatter in the areal extent of sediment cover since these areas are located only in the proglacial area of two of the largest glaciers, the Aletsch and the Fiescher glaciers. Both glaciers are located in very narrow and steep valleys, hence their glacier forefields are bedrock-dominated. The sediment cover at these elevations is thus lower than at the same elevations in the whole URB.

Our data support that proglacial areas in the Alps feature an intense availability of sediment (Maisch et al., 1999). In comparison to most other areas, they are very young (exposure max. 170 years) and glacial erosion and thus sediment production has been recently active. If recently deglaciated areas are subject to increased geomorphic activity (Carrivick et al., 2013) the availability of glacial sediment, recently analyzed in this and several other studies (review given by Heckmann et al., 2016), might pose a hazard through different geomorphic processes (Moore et al., 2009; Heckmann et al., 2016). The modeled sediment distribution in the URB could be further used to analyze the sediment cover of individual glacier forefields to improve the classification of sedimentary, bedrock and mixed sedimentary-rocky glacier forefields and beds, which is especially important to gain information about future hazards due to the ongoing deglaciation (Maisch et al., 1999; Zemp et al., 2005).

## 6. Conclusions

Bridging the gap between different spatial scales remains a major challenge in geomorphic research. This is especially true for the field of sediment budgets, where small scale ( $<10^2 \text{ km}^2$ ) investigations are primarily based on field work in individual headwater catchments, whereas large scale studies focus on the role of macro-sedimentary landforms in a regional context. Here we applied a combined field mapping and statistical modeling approach to fill this gap and to predict the location and spatial distribution of sediment and bedrock cover in the Upper Rhone Basin.

- Modeling approach and transferability: We compared different predictive modeling approaches, namely logistic regression, principal

component logistic regression, and generalized additive models. All tested models performed well, best prediction results with a high spatial and non-spatial transferability were achieved by a generalized additive model with five degrees of freedom. Our approach to train one model for a large scale, heterogeneous, mountain drainage basin, with a dataset representing this heterogeneity shows to be a suitable way to bridge the gap between large and small scale sediment budgets studies. However, the reference area mapped in the field has to represent the spatial heterogeneity of the large scale drainage basin, but we show that as few as c.  $50 \text{ km}^2$  of manual mapping could be sufficient.

- High-resolution model and its benefits: Our model of the spatial distribution of sediment and bedrock reveals that  $53.5 \pm 21.7\%$  of the Upper Rhone Basin are covered with sediment and predicts its location with  $2 \times 2 \text{ m}$  ground resolution. This dataset can serve as an important input for models of seismic wave propagation, hydropower management, and the assessment of sediment-related natural hazards in the Upper Rhone Basin. Moreover, future sediment budget studies will benefit from this data and might further explore its potential in estimating sedimentary volumes of individual landforms. In addition, the high spatial and non-spatial transferability of the model calls for an application to an even larger scale, e.g. to the entire Alps. This might reveal larger patterns of sediment distribution which are not discernible on the scale of one large scale catchment.
- Importance of small scale storage: Assuming a very conservative mean depth of 1–5 m for all sediment covered areas outside the main valley, we estimate that a volume of  $2.6\text{--}13 \text{ km}^3$  is trapped in low-order catchments. This finding underscores the relevance of small scale sediment storage in large scale sediment budgets. In the Upper Rhone Basin shallow diffusive hillslope storages at the ridges, upper and middle slopes alone constitute >50% of all sediment coverage. Sediment cover deposited mainly by rock falls, debris flows and fluvial processes at the lower slopes and the thalweg of tributaries comprises one third of relative sediment coverage. These results warrant a detailed volumetric quantification of the sediments stored in the large scale drainage basins that better include the entire spectrum of sedimentary landforms.
- Deglaciated areas and hazard: Areas that have deglaciated since the Little Ice Age show an elevated relative sediment coverage compared to the remaining catchment at similar elevations. Due to their recent exposure, these glacier forefields are characterized by low vegetation cover, and hence a reduced stability of the sediments trapped. Our data ultimately help assessing the natural hazard potential in a large alpine drainage basin, pinpointing the locations of loose sediments that might nourish catastrophic processes.

## Acknowledgements

The research was funded by the Geomorphology and Environmental Systems research group, University of Bonn (BZ9). The high-resolution DEM (©Swiss Federal Office of Topography) was provided by Martin Geilhausen and Patrick Laube from the Zurich University of Applied Sciences. The data on sediment storages in the Turtmannal were kindly made available by Jan-Christoph Otto. The field work in the Upper Rhone Basin, Switzerland, was supported by Christian Halla, Simon Terweh, Thomas Baumann and Gerrit Heinmüller. Finally, we thank Günther Prasicek for fruitful discussion, and Fritz Schlunegger and one anonymous reviewer for helpful comments that substantially improved the paper.

## Appendix A. Supplementary data

Supplementary data to this article can be found online at <https://doi.org/10.1016/j.geomorph.2017.11.026>.

## References

- Aguilera, A.M., Escabias, M., Valderrama, M.J., 2006. Using principal components for estimating logistic regression with high-dimensional multicollinear data. *Comput. Stat. Data Anal.* 50 (8), 1905–1924.

- Akaike, H., 1974. A new look at the statistical model identification. *IEEE Trans. Autom. Control* 19 (6), 716–723.
- Allen, T.I., Wald, D.J., 2009. On the use of high-resolution topographic data as a proxy for seismic site conditions (VS30). *Bull. Seismol. Soc. Am.* 99 (2A), 935–943.
- Atkinson, P., Jiskoot, H., Massari, R., Murray, T., 1998. Generalized linear modelling in geomorphology. *Earth Surf. Process. Landf.* 23 (13), 1185–1195.
- Baewert, H., Morche, D., 2014. Coarse sediment dynamics in a proglacial fluvial system (Fagge River, Tyrol). *Geomorphology* 218, 88–97.
- Ballantyne, C.K., 2002. Paraglacial geomorphology. *Quat. Sci. Rev.* 21 (18–19), 1935–2017.
- Beven, K.J., Kirkby, M.J., 1979. A physically based, variable contributing area model of basin hydrology/Un modèle à base physique de zone d'appel variable de l'hydrologie du bassin versant. *Hydrog. Sci. J.* 24 (1), 43–69.
- Blahut, J., van Westen, C.J., Sterlacchini, S., 2010. Analysis of landslide inventories for accurate prediction of debris-flow source areas. *Geomorphology* 119 (1–2), 36–51.
- Blöthe, J.H., Korup, O., 2013. Millennial lag times in the Himalayan sediment routing system. *Earth Planet. Sci. Lett.* 382, 38–46.
- Bowles, C.J., Cowgill, E., 2012. Discovering marine terraces using airborne LiDAR along the Mendocino-Sonoma coast, northern California. *Geosphere* 8 (2), 386–402.
- Brardinoni, F., Hassan, M.A., 2006. Glacial erosion, evolution of river long profiles, and the organization of process domains in mountain drainage basins of coastal British Columbia. *J. Geophys. Res. Earth* 111 (F1).
- Brenning, A., 2005. Spatial prediction models for landslide hazards: review, comparison and evaluation. *Nat. Hazards Earth Syst. Sci.* 5 (6), 853–862.
- Brenning, A., 2008. Statistical geocomputing combining R and SAGA: the example of landslide susceptibility analysis with generalized additive models. *SAGA—Seconds Out*, 19, pp. 23–32.
- Brenning, A., 2009. Benchmarking classifiers to optimally integrate terrain analysis and multispectral remote sensing in automatic rock glacier detection. *Remote Sens. Environ.* 113 (1), 239–247.
- Brenning, A., 2012. Spatial cross-validation and bootstrap for the assessment of prediction rules in remote sensing: The R package sperrorest. 2012 IEEE International Geoscience and Remote Sensing Symposium, pp. 5372–5375.
- Brocklehurst, S.H., Whipple, K.X., 2004. Hypsometry of glaciated landscapes. *Earth Surf. Process. Landf.* 29 (7), 907–926.
- Brunsdon, D., Thorne, J.B., 1979. Landscape sensitivity and change. *Trans. Inst. Br. Geogr.* 463–484.
- Burt, T., Allison, R.J., 2010. *Sediment Cascades: An Integrated Approach*. John Wiley & Sons.
- Caine, N., 1974. The geomorphic processes of the alpine environment. In: Ives, J.D., Barry, R.G. (Eds.), *Arctic and Alpine Environments*. Methuen, London, pp. 721–748.
- Carrivick, J.L., Geilhausen, M., Warburton, J., Dickson, N.E., Carver, S.J., Evans, A.J., Brown, L.E., 2013. Contemporary geomorphological activity throughout the proglacial area of an alpine catchment. *Geomorphology* 188, 83–95.
- Chander, G., Markham, B.L., Helder, D.L., 2009. Summary of current radiometric calibration coefficients for Landsat MSS, TM, ETM+, and EO-1 ALI sensors. *Remote Sens. Environ.* 113 (5), 893–903.
- Chorley, R.J., Kennedy, B.A., 1971. *Physical Geography: A Systems Approach*. Prentice-Hall, London.
- Church, M., Slaymaker, O., 1989. Disequilibrium of Holocene sediment yield in glaciated British-Columbia. *Nature* 337 (6206), 452–454.
- de Vente, J., Poesen, J., Arabkhedri, M., Verstraeten, G., 2007. The sediment delivery problem revisited. *Prog. Phys. Geogr.* 31 (2), 155–178.
- Evans, I.S., 2006. Allometric development of glacial cirque form: geological, relief and regional effects on the cirques of Wales. *Geomorphology* 80 (3–4), 245–266.
- Fawcett, T., 2006. An introduction to ROC analysis. *Pattern Recogn. Lett.* 27 (8), 861–874.
- Fischer, M., 2013. GLIMS Glacier Database. National Snow and Ice Data Center, Boulder, CO.
- Fischer, M., Huss, M., Barboux, C., Hoelzle, M., 2014. The new Swiss glacier inventory SGI2010: relevance of using high-resolution source data in areas dominated by very small glaciers. *Arct. Antarct. Alp. Res.* 46 (4), 933–945.
- Florineth, D., Schlüchter, C., 1998. Reconstructing the Last Glacial Maximum (LGM) ice surface geometry and flowlines in the central Swiss Alps. *Eclogae Geol. Helv.* 91 (3), 391–407.
- Fryirs, K., 2013. (Dis)connectivity in catchment sediment cascades: a fresh look at the sediment delivery problem. *Earth Surf. Process. Landf.* 38 (1), 30–46.
- Glade, T., 2005. Linking debris-flow hazard assessments with geomorphology. *Geomorphology* 66 (1–4), 189–213.
- Goetz, J.N., Guthrie, R.H., Brenning, A., 2011. Integrating physical and empirical landslide susceptibility models using generalized additive models. *Geomorphology* 129 (3–4), 376–386.
- Goetz, J.N., Brenning, A., Petschko, H., Leopold, P., 2015. Evaluating machine learning and statistical prediction techniques for landslide susceptibility modeling. *Comput. Geosci. UK* 81, 1–11.
- Götz, J., Otto, J.-C., Schrott, L., 2013. Postglacial sediment storage and rockwall retreat in a semi-closed inner-Alpine sedimentary basin (Gradenmoos, Hohe Tauern, Austria). *Geogr. Fis. Din. Quat.* 36, 63–80.
- Guisan, A., Weiss, S.B., Weiss, A.D., 1999. GLM versus CCA spatial modeling of plant species distribution. *Plant Ecol.* 143 (1), 107–122.
- Guzzetti, F., Reichenbach, P., Ardizzone, F., Cardinali, M., Galli, M., 2006. Estimating the quality of landslide susceptibility models. *Geomorphology* 81 (1–2), 166–184.
- Haeberli, W., Hoelzle, M., Paul, F., Zemp, M., 2007. Integrated monitoring of mountain glaciers as key indicators of global climate change: the European Alps. *Ann. Glaciol.* 46 (1), 150–160.
- Haeberli, W., Linsbauer, A., Cochachin, A., Salazar, C., Fischer, U.H., 2016. On the morphological characteristics of overdeepenings in high-mountain glacier beds. *Earth Surf. Process. Landf.* 41 (13), 1980–1990.
- Hallet, B., Hunter, L., Bogen, J., 1996. Rates of erosion and sediment evacuation by glaciers: a review of field data and their implications. *Glob. Planet. Chang.* 12 (1–4), 213–235.
- Hastie, T., 2015. GAM: Generalized Additive Models.
- Hastie, T., Tibshirani, R., 1990. *Generalized Additive Models*. 43. Chapman and Hall/CRC Press, London.
- Hastie, T., Tibshirani, R., Friedman, J., 2009. *The Elements of Statistical Learning - Additive Models, Trees, and Related Methods*. Springer.
- Heckmann, T., Gegg, K., Gegg, A., Becht, M., 2014. Sample size matters: investigating the effect of sample size on a logistic regression susceptibility model for debris flows. *Nat. Hazards Earth Syst. Sci.* 14 (2), 259–278.
- Heckmann, T., McColl, S., Morche, D., 2016. Retreating ice: research in pro-glacial areas matters. *Earth Surf. Process. Landf.* 41 (2), 271–276.
- Hengl, T., Heuvelink, G.B.M., Stein, A., 2004. A generic framework for spatial prediction of soil variables based on regression-kriging. *Geoderma* 120 (1–2), 75–93.
- Hijmans, R.J., 2014. *Raster: Geographic Data Analysis and Modeling*.
- Hinderer, M., 2001. Late Quaternary denudation of the Alps, valley and lake fillings and modern river loads. *Geodin. Acta* 14 (4), 231–263.
- Hinderer, M., 2012. From gullies to mountain belts: a review of sediment budgets at various scales. *Sediment. Geol.* 280, 21–59.
- Hinderer, M., Kastowski, M., Kamelger, A., Bartolini, C., Schlunegger, F., 2013. River loads and modern denudation of the Alps - a review. *Earth-Sci. Rev.* 118, 11–44.
- Hoffmann, T., 2015. Sediment residence time and connectivity in non-equilibrium and transient geomorphic systems. *Earth-Sci. Rev.* 150, 609–627.
- Hoffmann, T., Müller, T., Johnson, E.A., Martin, Y.E., 2013. Postglacial adjustment of steep, low-order drainage basins, Canadian Rocky Mountains. *J. Geophys. Res. Earth* 118 (4), 2568–2584.
- Hoffmann, U., Hoffmann, T., Jurasiczki, G., Glatzel, S., Kuhn, N.J., 2014. Assessing the spatial variability of soil organic carbon stocks in an alpine setting (Grindelwald, Swiss Alps). *Geoderma* 232, 270–283.
- Hollander, M., Wolfe, D.A., 1999. *Nonparametric Statistical Methods*. John Wiley & Sons, Inc.
- Hooke, R.L., 1991. Positive feedbacks associated with erosion of glacial cirques and overdeepenings. *Geol. Soc. Am. Bull.* 103 (8), 1104–1108.
- Hosmer, D.W., Lemeshow, S., Sturdivant, R.X., 2013. *Applied Logistic Regression*. Wiley Series in Probability and Statistics. Wiley, New York.
- Huss, M., Bookhagen, B., Huggel, C., Jacobsen, D., Bradley, R.S., Clague, J.J., Vuille, M., Buytaert, W., Cayan, D.R., Greenwood, G., Mark, B.G., Millner, A.M., Weingartner, R., Winder, M., 2017. Toward mountains without permanent snow and ice. *Earth's Future*, 5, pp. 1–18.
- Ivy-Ochs, S., Schäfer, J., Kubik, P.W., Synal, H.A., Schlüchter, C., 2004. Timing of deglaciation on the northern Alpine foreland (Switzerland). *Eclogae Geol. Helv.* 97 (1), 47–55.
- Ivy-Ochs, S., Kerschner, H., Reuther, A., Maisch, M., Sailer, R., Schäfer, J., Kubik, P.W., Synal, H.-A., Schlüchter, C., 2006. The timing of glacier advances in the northern European Alps based on surface exposure dating with cosmogenic  $^{10}\text{Be}$ ,  $^{26}\text{Al}$ ,  $^{36}\text{Cl}$ , and  $^{21}\text{Ne}$ . *Geol. Soc. Am. Spec. Pap.* 415, 43–60.
- Jaboyedoff, M., Derron, M.-H., 2005. A new method to estimate the infilling of alluvial sediment of glacial valleys using a sloping local base level. *Geogr. Fis. Din. Quat.* 28 (1), 37–46.
- Jäckli, H., 1957. *Gegenwartsgeschichte des bündnerischen Rheingebietes: ein Beitrag zur exogenen Dynamik alpiner Gebirgslandschaften*. Kümmery & Frey, Geograph. Verlag.
- James, G., Witten, D., Hastie, T., Tibshirani, R., 2013. *An Introduction to Statistical Learning: With Applications in R*. Springer Texts in Statistics. 6. Springer, New York.
- Jordan, P., Slaymaker, O., 1991. Holocene sediment production in Lillooet River basin, British Colombia: a sediment budget approach. *Géog. Phys. Quatern.* 45 (1), 45–57.
- Kahle, H.G., Geiger, A., Bürki, B., Gubler, E., Marti, U., Wirth, B., Rothacher, M., Gurtner, W., Beutler, G., Bauersima, I., 1997. Recent crustal movements, geoid and density distribution: contribution from integrated satellite and terrestrial measurements. Results of the National Research Program. 20, pp. 251–259.
- Kaiser, H.F., 1958. The varimax criterion for analytic rotation in factor-analysis. *Psychometrika* 23 (3), 187–200.
- Kelly, M.A., Buoncristiani, J.F., Schlüchter, C., 2004. A reconstruction of the last glacial maximum (LGM) ice-surface geometry in the western Swiss Alps and contiguous Alpine regions in Italy and France. *Eclogae Geol. Helv.* 97 (1), 57–75.
- Korup, O., Schlunegger, F., 2007. Bedrock landsliding, river incision, and transience of geomorphic hillslope-channel coupling: evidence from inner gorges in the Swiss Alps. *J. Geophys. Res. Earth* 112 (F3).
- Kühni, A., Pfiffner, O.A., 2001. The relief of the Swiss Alps and adjacent areas and its relation to lithology and structure: topographic analysis from a 250-m DEM. *Geomorphology* 41 (4), 285–307.
- Lane, S.N., Bakker, M., Gabbud, C., Micheletti, N., Saugy, J.N., 2017. Sediment export, transient landscape response and catchment-scale connectivity following rapid climate warming and Alpine glacier recession. *Geomorphology* 277, 210–227.
- Luoto, M., Hjort, J., 2005. Evaluation of current statistical approaches for predictive geomorphological mapping. *Geomorphology* 67 (3–4), 299–315.
- Maisch, M., 2000. *Die Gletscher der Schweizer Alpen: Gletscherhochstand 1850, aktuelle Vergletscherung, Gletscherschwund-Szenarien*. vdf, Hochsch.-Verl. an der ETH, Zürich.
- Maisch, M., Haeberli, W., Hoelzle, M., Wenzel, J., 1999. Occurrence of rocky and sedimentary glacier beds in the Swiss Alps as estimated from glacier-inventory data. *Ann. Glaciol.* 28 (1), 231–235.
- Marmion, M., Hjort, J., Thuiller, W., Luoto, M., 2008. A comparison of predictive methods in modelling the distribution of periglacial landforms in Finnish Lapland. *Earth Surf. Process. Landf.* 33 (14), 2241–2254.
- McColl, S.T., 2012. Paraglacial rock-slope stability. *Geomorphology* 153, 1–16.

- Messenzehl, K., Hoffmann, T., Dikau, R., 2014. Sediment connectivity in the high-alpine valley of Val Muschauns, Swiss National Park - linking geomorphic field mapping with geomorphometric modelling. *Geomorphology* 221, 215–229.
- Messenzehl, K., Meyer, H., Otto, J.-C., Hoffmann, T., Dikau, R., 2017. Regional-scale controls on the spatial activity of rockfalls (Turtmann Valley, Swiss Alps) - a multivariate modeling approach. *Geomorphology* 287, 29–45.
- Mey, J., Scherler, D., Zeilinger, G., Strecker, M.R., 2015. Estimating the fill thickness and bedrock topography in intermontane valleys using artificial neural networks. *J. Geophys. Res. Earth* 120 (7), 1301–1320.
- Milliman, J.D., Svitshi, J.P., 1992. Geomorphic/tectonic control of sediment discharge to the ocean: the importance of small mountainous rivers. *J. Geol.* 525–544.
- Molnar, P., England, P., 1990. Late Cenozoic uplift of mountain ranges and global climate change: chicken or egg? *Nature* 346, 29–34.
- Montgomery, D.R., 2002. Valley formation by fluvial and glacial erosion. *Geology* 30 (11), 1047–1050.
- Moore, R.D., Fleming, S.W., Menounos, B., Wheate, R., Fountain, A., Stahl, K., Holm, K., Jakob, M., 2009. Glacial change in western North America: influences on hydrology, geomorphic hazards and water quality. *Hydrol. Process.* 23 (1), 42–61.
- Norton, K.P., Abbuhl, L.M., Schlunegger, F., 2010. Glacial conditioning as an erosional driving force in the Central Alps. *Geology* 38 (7), 655–658.
- O'Callaghan, J.F., Mark, D.M., 1984. The Extraction of Drainage Networks From Digital Elevation Data. *Comput Vision Graph.* 28(3) pp. 323–344.
- Otto, J.-C., Götz, J., Schrott, L., 2008. Sediment storage in Alpine sedimentary systems - quantification and scaling issues. *IAHS Publ.* 325, 258–265.
- Otto, J.-C., Schrott, L., Jabyedoff, M., Dikau, R., 2009. Quantifying sediment storage in a high alpine valley (Turtmannal, Switzerland). *Earth Surf. Process. Landf.* 34 (13), 1726–1742.
- Penck, A., 1905. Glacial features in the surface of the Alps. *J. Geol.* 13 (1), 1–19.
- Petschko, H., Bell, R., Glade, T., Brenning, A., 2012. Landslide susceptibility modeling with generalized additive models—facing the heterogeneity of large regions. In: Erik Eberhardt, E., Froese, C., Turner, K., Leroueil, S. (Eds.), *Landslides and Engineered Slopes: Protecting Society Through Improved Understanding*. CRC Press, London, pp. 769–775.
- Petschko, H., Brenning, A., Bell, R., Goetz, J., Glade, T., 2014. Assessing the quality of landslide susceptibility maps - case study Lower Austria. *Nat. Hazards Earth Syst. Sci.* 14 (1), 95–118.
- Pfiffner, O.A., Heitzmann, P., Lehner, P., Frei, W., Pugin, A., Felber, M., 1997. Incision and Backfilling of Alpine valleys: Pliocene, Pleistocene and Holocene Processes. Deep Structure of the Swiss Alps: Results of NRP. 20 pp. 265–288.
- Phillips, J.D., 1986. Sediment storage, sediment yield, and time scales in landscape denudation studies. *Geogr. Anal.* 18 (2), 161–167.
- Phillips, J.D., 1991. Fluvial sediment budgets in the North Carolina Piedmont. *Geomorphology* 4 (3), 231–241.
- Phillips, J.D., 1999. Earth Surface Systems: Complexity, Order, and Scale. The Natural Environment. Blackwell, Malden, Mass.
- Phillips, J.D., 2003. Alluvial storage and the long-term stability of sediment yields. *Basin Res.* 15 (2), 153–163.
- Prasicek, G., Otto, J.-C., Montgomery, D.R., Schrott, L., 2014. Multi-scale curvature for automated identification of glaciated mountain landscapes. *Geomorphology* 209, 53–65.
- Preusser, F., Reitner, J.M., Schlüchter, C., 2010. Distribution, geometry, age and origin of overdeepened valleys and basins in the Alps and their foreland. *Swiss J. Geosci.* 103 (3), 407–426.
- Revelle, W., 2015. Psych: Procedures for Personality and Psychological Research. Northwestern University, Evanston, Illinois.
- Rosselli, A., Olivier, R., 2003. Modélisation gravimétrique 2.5 D et cartes des isohypses au 1: 100'000 du substratum rocheux de la Vallée du Rhône entre Villeneuve et Brig (Suisse).
- Sass, O., 2006. Determination of the internal structure of alpine talus deposits using different geophysical methods (Lechtaler Alps, Austria). *Geomorphology* 80 (1–2), 45–58.
- Sass, O., 2007. Bedrock detection and talus thickness assessment in the European Alps using geophysical methods. *J. Appl. Geophys.* 62 (3), 254–269.
- Schlatter, A., Schneider, D., Geiger, A., Kahle, H.G., 2005. Recent vertical movements from precise levelling in the vicinity of the city of Basel, Switzerland. *Int. J. Earth Sci.* 94 (4), 507–514.
- Schlüchter, C., 2004. The Swiss glacial record - a schematic summary. In: Ehlers, J., Gibbard, P.L. (Eds.), *Quaternary Glaciations Extent and Chronology Part I: Europe. Developments in Quaternary Sciences*. Elsevier, Amsterdam, pp. 413–418.
- Schlummer, M., Hoffmann, T., Dikau, R., Eickmeier, M., Fischer, P., Gerlach, R., Holzkamper, J., Kalis, A.J., Kretschmer, I., Lauer, F., Maier, A., Meesenburg, J., Meurers-Balke, J., Munch, U., Patzold, S., Steininger, F., Stobbe, A., Zimmermann, A., 2014. From point to area: upscaling approaches for Late Quaternary archaeological and environmental data. *Earth-Sci. Rev.* 131, 22–48.
- Schlunegger, F., Hinderer, M., 2003. Pleistocene/Holocene climate change, re-establishment of fluvial drainage network and increase in relief in the Swiss Alps. *Terra Nova* 15 (2), 88–95.
- Schlunegger, F., Norton, K.P., 2013. Water versus ice: the competing roles of modern climate and Pleistocene glacial erosion in the Central Alps of Switzerland. *Tectonophysics* 602, 370–381.
- Schmid, S.M., Fügenschuh, B., Kissling, E., Schuster, R., 2004. Tectonic map and overall architecture of the Alpine orogen. *Eclogae Geol. Helv.* 97 (1), 93–117.
- Schrott, L., Hufschmidt, G., Hankammer, M., Hoffmann, T., Dikau, R., 2003. Spatial distribution of sediment storage types and quantification of valley fill deposits in an alpine basin, Reintal, Bavarian Alps, Germany. *Geomorphology* 55 (1), 45–63.
- Schumm, S.A., 1977. *The Fluvial System*. Wiley, New York.
- Sing, T., Sander, O., Beerewinkel, N., Lengauer, T., 2005. ROCR: visualizing classifier performance in R. *Bioinformatics* 21 (20), 3940–3941.
- Slaymaker, O., 1991. Mountain geomorphology: a theoretical framework for measurement programmes. *Catena* 18 (5), 427–437.
- Slaymaker, O., 2006. Towards the identification of scaling relations in drainage basin sediment budgets. *Geomorphology* 80 (1–2), 8–19.
- Steger, S., Bell, R., Petschko, H., Glade, T., 2015. Evaluating the effect of modelling methods and landslide inventories used for statistical susceptibility modelling. *Engineering Geology for Society and Territory. vol. 2*. Springer, pp. 201–204.
- Steger, S., Brenning, A., Bell, R., Petschko, H., Glade, T., 2016. Exploring discrepancies between quantitative validation results and the geomorphic plausibility of statistical landslide susceptibility maps. *Geomorphology* 262, 8–23.
- Straumann, R.K., Korup, O., 2009. Quantifying postglacial sediment storage at the the mountain-belt scale. *Geology* 37 (12), 1079–1082.
- Tunncliffe, J.F., Church, M., 2011. Scale variation of post-glacial sediment yield in Chilliwack Valley, British Columbia. *Earth Surf. Process. Landf.* 36 (2), 229–243.
- Tunncliffe, J., Church, M., Clague, J.J., Feathers, J.K., 2012. Postglacial sediment budget of Chilliwack Valley, British Columbia. *Earth Surf. Process. Landf.* 37 (12), 1243–1262.
- Valla, P.G., van der Beek, P.A., Carcailliet, J., 2010a. Dating bedrock gorge incision in the French Western Alps (Ecrins-Pelvoux massif) using cosmogenic 10Be. *Terra Nova* 22 (1), 18–25.
- Valla, P.G., van der Beek, P.A., Lague, D., 2010b. Fluvial incision into bedrock: insights from morphometric analysis and numerical modeling of gorges incising glacial hanging valleys (Western Alps, France). *J. Geophys. Res. Earth* 115.
- Van den Berg, F., Schlunegger, F., Akcar, N., Kubik, P., 2012. 10Be-derived assessment of accelerated erosion in a glacially conditioned inner gorge, Entlebuch, Central Alps of Switzerland. *Earth Surf. Process. Landf.* 37 (11), 1176–1188.
- Vernon, A.J., van der Beek, P.A., Sinclair, H.D., Rahn, M.K., 2008. Increase in late Neogene denudation of the European Alps confirmed by analysis of a fission-track thermochronology database. *Earth Planet. Sci. Lett.* 270 (3–4), 316–329.
- Vogelmann, J.E., Howard, S.M., Yang, L.M., Larson, C.R., Wylie, B.K., Van Driel, N., 2001. Completion of the 1990s National Land Cover Data set for the conterminous United States from Landsat Thematic Mapper data and Ancillary data sources. *Photogramm. Eng. Remote Sens.* 67 (6), 650–662.
- Walling, D.E., 1983. The sediment delivery problem. *J. Hydrol.* 65 (1–3), 209–237.
- Weiss, A.D., 2000. Topographic Position and Landforms Analysis, Poster Presentation, ESRI Users Conference, San Diego, CA.
- Whipple, K.X., 2009. The influence of climate on the tectonic evolution of mountain belts. *Nat. Geosci.* 2 (2), 97–104.
- Zemp, M., Käab, A., Hoelze, M., Haeberli, W., 2005. GIS-based modelling of glacial sediment balance. *Z. Geomorphol. Suppl.* 138, 113–129.
- Zemp, M., Paul, F., Hoelze, M., Haeberli, W., 2008. Glacier fluctuations in the European Alps, 1850–2000. In: Orlove, B., Wiegandt, E., Luckman, B.H. (Eds.), *Darkening Peaks – Glacier Retreat, Science, and Society*. University of California Press, Berkeley, US, pp. 152–167.
- Zhang, X., Drake, N.A., Wainwright, J., 2004. Scaling issues in environmental modelling. In: Wainwright, J., Mulligan, M. (Eds.), *Environmental Modelling: Finding Simplicity in Complexity*. John Wiley & Sons, Ltd., London, pp. 319–334.
- Zimmermann, M., Haeberli, W., 1993. Climatic change and debris flow activity in high-mountain areas—a case study in the Swiss Alps. *Catena Suppl.* 22, 59–72.